GSA Data Repository 2016328

The cause of Late Cretaceous cooling: A multi-model/proxy comparison

Clay R. Tabor[1,2], Christopher J. Poulsen[1], Daniel J. Lunt[3], Nan A. Rosenbloom[2], Bette L. Otto-Bliesner[2], Paul J. Markwick[4], Esther C. Brady[2], Alexander Farnsworth[3], and Ran Feng[2]

[1] Department of Earth and Environmental Sciences, University of Michigan, 2534 C. C. Little Building, 1100 North University Ave, Ann Arbor, MI 48109

[2] National Center for Atmospheric Research, 1850 Table Mesa Dr, Boulder, CO 80305

[3] School of Geographic Sciences, University of Bristol, University Road, Clifton, Bristol BS8 1SS

[4] Getech, Kitson House, Elmete Hall, Elmete Lane, Leeds, LS8 2LJ

GSA DATA REPOSITORY

MODEL DESCRIPTIONS

CCSM4

We use the Community Climate System Model version 4 (CCSM4) maintained at the National Center for Atmospheric Research (NCAR). Our model component-set includes the Community Atmospheric Model version 4 (CAM4), the Community Land Model version 4 with dynamic vegetation (CLM4-DGVM), the Parallel Ocean Project model version 2 (POP2), and the Community Sea Ice model version 4 (CICE4). Additional details on the model components and performance can be found in Gent et al. (2011), and information on the DGVM is

documented in Levis et al. (2004). The ocean and sea ice models run on a rotated poles grid at roughly 1° resolution with 60 vertical ocean levels. The atmosphere and land-surface models run on a finite-volume grid of 1.9×2.5°, and the atmosphere has 28 vertical levels. We run CAM4 with the Bulk Aerosol Model (BAM), a prognostic aerosol model, with aerosol concentrations and types adjusted for the Cretaceous using a method similar to Heavens et al. (2012). Here, aerosol data come from pre-industrial datasets converted into hemispherically symmetric, monthly zonal average aerosols distributions masked independently to land and sea. In addition, we add the land black carbon emissions from 62.5°N/S to all latitudes further poleward to reflect the greater vegetation cover and fire potential at high latitudes during the Cretaceous (Upchurch et al., 1998). We run all simulations for 1500 years with all model components active and synchronously coupled.

HadCM3L

We also use the Hadley Centre Model (HadCM), developed by the UK Met Office. For this study, we implement HadCM3L version 4.5, which contains dynamic atmosphere, ocean, land, and sea ice components on a 2.5x3.75° grid. The ocean and atmosphere have 19 and 20 vertical levels, respectively. Description of the similar HadCM3 model is documented in Gordon et al. (Gordon et al., 2000). We couple HadCM3L with the Top-down Representation of Interactive Foliage and Flora Including Dynamics (TRIFFID) model with the land surface scheme MOSES 2.1 to simulate dynamic vegetation (Cox, 2001). We run the HadCM3 experiments in 4 phases:

1. 50 years with 280 ppm CO_2 and bare-ground

2. 319 years of either 560 or 1120 ppm CO_2 with TRIFFID turned on
3. 53 years with the addition of prescribed lakes
4. 1000 years with barotropic ocean flow enabled to allow non-zero vertically integrated ocean flow

For additional details on HadCM3L initialization and spin-up see Lunt et al. (2015).

MODELS SETUP

Simulations use the paleogeographic reconstructions of Getech Plc. Following model standard practices and for improved stability, we apply model specific smoothing to the topography. For both models, we adjust total TSI for the Cenomanian (CEN) and Maastrichtian (MAA) based on the equation of Gough (1981). We prescribe CO_2 concentrations as either 4x (1120 ppm) or 2x preindustrial (560 ppm). All other GHG concentrations are set to preindustrial values of 790 ppb for CH_4, 275 ppb for N_2O, and no CFCs. The orbit configuration is set to present-day. Vegetation plant functional types are model defaults; we make no adjustments for the Cretaceous. All simulations run long enough for the upper ocean to reach near-equilibrium; however, the deep ocean continues to adjust. As a result, we focus only on surface conditions.

ENERGY BALANCE CALCULATIONS

We use the zonal mean energy balance decomposition method of Heinemann (2009), which was subsequently adopted and modified by Lunt et al. (2012), and Hill et al. (2014), to explore the mechanisms responsible for surface temperature change in the Late Cretaceous with changes in paleogeography and CO_2. This method assumes incoming shortwave balances with outgoing longwave and that local imbalances are due to changes heat convergence, using the

following relationship:

$$\frac{S_0}{4}(1-\alpha)+H=\varepsilon\sigma T^4 \text{ . (1)}$$

Here, S_0 is TSI, α is albedo, H is meridional heat convergence, ε is emissivitiy, σ (5.67×10^{-8} $Wm^{-2}K^{-4}$) is the Stefan-Boltzmann constant, and T is surface temperature. With the exception of σ, values in equation (1) come from zonal averages of Earth system model outputs. We can rewrite equation (1) with respect to surface temperature as:

$$T=\left(\frac{1}{\varepsilon\sigma}\left(\frac{S_0}{4}(1-\alpha)+H\right)^{0.25}\right)\equiv E(\varepsilon,\alpha,H) \text{ . (2)}$$

By substituting variables from different simulations and differencing them, we can deconstruct the various contributions to the change in surface temperature. We illustrate this below:

$$\Delta T_{emm}=E(\varepsilon,\alpha,H)-E(\varepsilon',\alpha,H) \text{ . (3)}$$

$$\Delta T_{alb}=E(\varepsilon,\alpha,H)-E(\varepsilon,\alpha',H) \text{ . (4)}$$

$$\Delta T_{tran}=E(\varepsilon,\alpha,H)-E(\varepsilon,\alpha,H') \text{ . (5)}$$

where ΔT_{emm}, ΔT_{alb}, and ΔT_{tran} are contributions from emissivity, albedo, and heat convergence to surface temperature change, and primes represent the zonal averages from the simulations being compared. The combination of surface temperature changes due to emissivity, albedo, and heat convergence sum to approximate the total surface temperature response:

$$\Delta T_{total}\cong\Delta T_{emm}+\Delta T_{alb}+\Delta T_{tran} \text{ . (6)}$$

This technique can be used to further decompose the climate contributions to surface temperature.

PROXY DATA

As mentioned in the main text, SST proxy values represent location and age averages. Method uncertainties only accounts for calibration uncertainties. We apply these uncertainties to every averaged data point. The range in values from a particular age and site are often significantly greater than the calibration uncertainties. Therefore, uncertainties represent minimum estimates.

Point locations are consistently rotated back in time from their present-day sampling locations to the CEN and MAA using the plate reconstructions from Getech Plc. Occasionally, the coarse model resolutions result in marine proxy paleo-locations over land instead of water. In these situations, we select the nearest model ocean location to represent the SST value.

To create more representative latitudinal SST gradients, Gaussian fits of the proxies include an adjustment for the deviation of the SSTs from the zonal mean based on model-simulated longitudinal heterogeneity. For example, if an equatorial proxy location has a model simulated SST of 30°C and a model zonal mean equatorial SST of 35°C, then 5°C are added to the proxy value so that it is in better agreement with the zonal average. This technique assumes that model longitudinal variability is robust regardless of mean SSTs.

We investigate the statistical similarity between the temperature gradients of our CEN and MAA datasets using an F-test. An F-test determines if the variance of multiple datasets are statistically different from each other. To standardize the data, we first remove the global means of the Gaussian fitting procedure (Fig. 2d). Then, we apply an F-test to test the hypothesis that the spread of residual SSTs between the CEN and MAA are statistically distinct. Our results produce a p-value equal to 0.39, which suggests that SST variations, except for the means

between datasets, are not robust.

Seawater $\delta^{18}O$

We assume a mean $\delta^{18}O_{sw}$ of -1 $^{0}/_{00}$ VSMOW, based on the assumption of an ice-free world (Shackleton and Kennett, 1975). This assumption is widely used in Cretaceous SST reconstructions (e.g. Huber et al., 2002; Friedrich et al., 2012); however, debate remains about the potential for glaciation in the Late Cretaceous (e.g. Miller et al., 2005). A significant increase in land-ice would require less cooling in the MAA from $\delta^{18}O$ records but is not considered further in this study.

$\delta^{18}O_{sw}$ has significant regional variability in both the modern and Late Cretaceous (Zhou et al., 2008). To account for this variability, we use zonal average salinity from the model outputs with the present-day salinity/$\delta^{18}O_{sw}$ relationship of Broecker (1989). This simple linear relationship follows:

$$\delta^{18}O_w = 0.5(PSU) - 17.12 \quad (7)$$

where PSU stands for positive salinity units. In our simulations, mean ocean salinity starts at 35 PSU, which is equivalent to present-day. While not perfect, we prefer this relationship to the commonly employed present-day latitudinal $\delta^{18}O_{sw}$ correction by Zachos et al. (1994), because it indirectly accounts for precipitation and evaporation, and does not make present-day assumptions about the latitudinal distribution of $\delta^{18}O_{sw}$ (Poulsen et al., 1999). Still, this technique is inferior to model experiments that include water isotope tracking (e.g. Zhou et al., 2008).

Planktonic Foraminifera

We calculate SSTs from $\delta^{18}O$ measurements of planktonic foraminifera using the calibration of Erez and Luz (1983) and a conversion to VSMOW of -0.22‰ (Bemis et al., 1998). This calibration has been widely used for foraminifera temperature reconstructions and proven accurate for a wide range of temperatures. Temperatures are calculated using the polynomial:

$$T(°C) = 16.998 - 4.52[\delta^{18}O_c - \delta^{18}O_{sw}] + 0.028[\delta^{18}O_c - \delta^{18}O_{sw}]^2 \quad (8)$$

where $\delta^{18}O_c$ is the $\delta^{18}O$ of sample calcite.

Diagenetic alteration is a potential issue for foraminifera, causing them to pickup post-depositional temperature signals from the ocean floor (e.g. Pearson et al., 2001; Norris et al., 2002). It is likely that some of the foraminifera presented in this study suffer from such alteration given the sample descriptions, relatively cool tropical SSTs, and disagreement with other SST proxy values. However, given the paucity of records and uncertainty in other included proxy techniques such as TEX_{86} (e.g. Taylor et al., 2013), we opt to include all planktonic foraminifera data. For comparison, we include zonal SST reconstructions without foraminifera as well (Fig. DR8, DR9, DR10). Even though removal of foraminifera leads to warmer tropical SST reconstructions, it does not significantly change the magnitude of cooling from the CEN to the Maa, which is the main focus of this study. We assign an uncertainty of $\pm$2.9°C for planktonic foraminifera based on Holocene core-top data from Crowley and Zachos (Crowley and Zachos, 2000) and to be consistent with the work of Upchurch (2015).

Shells and Others

We use the $\delta^{18}O$ to temperature conversion of Anderson and Arthur (1983) for both

aragonite and calcite of shells of mollusks, bivalves, brachiopods, and belemnite rosta based on its prevalent use in the proxy source literature (Grossman, 2012). The equation is:

$$T(°C) = 16.4 - 4.14(\delta^{18}O_{c/a} - \delta^{18}O_{sw}) + 0.13(\delta^{18}O_{c/a} - \delta^{18}O_{sw})^2 \text{ . (9)}$$

where $\delta^{18}O_{c/a}$ is the $\delta^{18}O$ of sample calcite or aragonite. Like foraminifera, shells are prone to alteration (Steuber et al., 1999). We include all records here for completeness. We also show comparisons with shell SST proxies omitted (Fig. DR8, DR9, DR10). We apply an uncertainty of ±1.6 based on 1σ of a mollusk calibration by Grossman and Ku (1986) as in Upchurch et al. (2015).

Tooth Enamel $\delta^{18}O$

Our SST proxy compilation includes phosphate $\delta^{18}O$ records from fish tooth enamel, most of which were originally compiled by Pucéat et al. (2007). These records are considered more resistant to diagenetic alteration than foraminifera or shells, and were previously used by Pucéat et al. (2007) to argue for a near-modern latitudinal SST gradient in the Cretaceous, in contrast to reconstructions from foraminifera that suggested a shallower latitudinal SST gradient (e.g. Huber et al., 2002). Recently, there have been several recalibrations of the phosphate $\delta^{18}O$ temperature relationship. Here, we use the most recent calibration by Lecuyer et al. (2013):

$$T(°C) = 117.4 - 4.5(\delta^{18}O_{PO4} - \delta^{18}O_{sw}) \text{ . (10)}$$

where $\delta^{18}O_{PO4}$ is the $\delta^{18}O$ of sample phosphate. This calibration results in SSTs that are several degrees warmer than the calibration by Pucéat et al. (2007) and several degrees cooler than the recent calibration by Pucéat et al. (2010). However, the magnitude of offset between calibrations remains quite similar over the range of $\delta^{18}O_{PO4}$ values. Therefore, while the absolute temperature

reconstructions differ depending on the chosen calibration, the difference between the CEN and MAA records is small. In addition, the calibration of Lecuyer et al. (2013) benefits from the smallest uncertainty of ±1.2°C, which we apply to all tooth enamel SST values.

TEX_{86}

TEX_{86} is a relatively new SST proxy method based on the ratio of different glycerol dialkyl glycerol tetraethers (GDGTs) with 86 carbons, which comprise membrane lipids in marine Crenarchaeota (Schouten et al., 2002). It has the benefit of not relying on $\delta^{18}O_{sw}$ assumptions. Here, we use the calibration of Kim et al. (2010) TEX_{86}^{H}, which provides the smallest error in warm climate conditions. The equation is:

$$T(°C) = 68.4 \log(TEX_{86}) + 38.6 \text{ . (11)}$$

Modern calibration by Kim et al. (2010) show an uncertainty of ±2.5°C, which we use in our model/proxy comparison.

We include the high-latitude MAA TEX_{86}^{H} SST value from Jenkyns et al. (2004) in our tables and plots for reference but do not include it in our analyses. We find, like several former studies (Davies et al., 2009; Spicer and Herman, 2010; Upchurch et al., 2015), that this value represents an extreme outlier from other proxy data and model results. Inclusion of this data point significantly skews our results, because it is the only available Arctic MAA SST value. Based on our other findings, it requires roughly 10°C warming from 50°N to 80°N, for which we have no physical basis.

GSA DATA REPOSITORY FIGURE CAPTIONS

Figure DR1. Getech Plc CEN and MAA paleogeography with marine proxy locations.

188 Figure DR2: Individual model simulated Late Cretaceous mean annual surface temperatures and
189 temperature responses to changes in paleogeography and CO_2 concentration. Row 1 shows
190 CCSM4 mean annual surface temperatures from CEN4x (A), MAA4x (B), and MAA2x (C).
191 Row 2 shows HadCM3L mean annual surface temperatures from CEN4x (D), MAA4x (E), and
192 MAA2x (F). Row 3 shows CCSM4 mean annual surface temperature differences between
193 CEN4x and MAA4x (G), MAA4x and MAA2x (H), and CEN4x and MAA2x (I). Row 4 shows
194 HadCM3L mean annual surface temperature differences between CEN4x and MAA4x (J),
195 MAA4x and MAA2x (K), and CEN4x and MAA2x (L). The large-scale surface temperature
196 patterns are quite similar for both models.
197 Figure DR3. Late Cretaceous mean annual total cloud cover and anomalies. Column 1 shows the
198 model total cloud cover from A) CEN4x, B) MAA4x, and C) MAA2x. Column 2 shows the
199 difference in total cloud cover between D) CEN4x and MAA4x, E) MAA4x and MAA2x, and F)
200 CEN4x and MAA2x. Column 3 shows the total cloud cover anomalies between CCSM4 and
201 HadCM3L for G) CEN4x, H) MAA4x, and I) MAA2x. Clouds remain one of the largest
202 uncertainties in climate models. Both models show similar cloud patterns for all model
203 configurations. However, the range of cloud cover between regions is more pronounced in
204 HadCM3L than CCSM4. The configuration of the CCSM4 aerosols for paleoclimate might be
205 partly responsible for the discrepancies in cloud magnitude.
206 Figure DR4. Late Cretaceous mean annual surface albedo and anomalies. Column 1 shows the
207 model surface albedo from A) CEN4x, B) MAA4x, and C) MAA2x. Column 2 shows the
208 difference in surface albedo between D) CEN4x and MAA4x, E) MAA4x and MAA2x, and F)

CEN4x and MAA2x. Column 3 shows the surface albedo anomalies between CCSM4 and HadCM3L for G) CEN4x, H) MAA4x, and I) MAA2x. In the high-latitudes, CCSM4 simulates higher surface albedos than HadCM3L due to differences in sea ice cover and vegetation. CCSM4 tends to produce more sea in the Arctic than HadCM3L, which leads to greater shortwave reflection, especially in the spring and fall. CCSM4 also grows shorter, less dense vegetation than HadCM3L in the polar regions. A lower vegetation and reduced canopy allows for more snow cover of vegetation, which raises the albedo. Tall, dense Antarctic vegetation suggested by paleobotantical reconstructions is not simulated in CCSM4 (e.g. Upchurch et al., 1998). Modification of the vegetation model will be an important step in our future work, as some research shows vegetation can help remedy model/proxy LST discrepancies (e.g. Otto-Bliesner and Upchurch, 1998; Zhou et al., 2012).

Figure DR5. Zonal mean annual SST responses to changing topography and decreasing CO_2 for both CCSM4 and HadCM3L models. Comparison of CCSM4 and HadCM3L outputs highlight the similarities in surface temperature response.

Figure DR6. Decomposition of the simulated changes in zonal mean surface temperature into contributions from heat convergence (red), emissivity (green), albedo (blue), and TSI (yellow) for A) CCSM4 and B) HadCM3L changes in geography, C) CCSM4 and D) HadCM3L changes in CO_2, and E) CCSM4 and F) HadCM3L changes in both geography and CO_2. See Data Repository for details on energy balance calculations.

Figure DR7. Seasonal sea ice exists in all 4x PI CO_2 simulations in agreement with some proxies that find evidence for Arctic sea ice during peak Cretaceous warmth (Davies et al., 2009). The

230 Arctic experiences an increase in sea ice concentration from the CEN to MAA because the
231 Arctic becomes more restricted in the Maa. With a reduction in CO_2, a significant amount of
232 perennial sea ice forms in the Arctic while Antarctic sea ice remains mostly seasonal. This
233 contrast in sea ice between hemispheres is similar to present-day where the restricted Arctic
234 promotes retention of sea ice, and the open ocean Antarctic allows the equator drift and wasting
235 of sea ice.

236 In all experiments, CCSM4 produces greater Arctic sea ice cover and less Antarctic sea
237 ice cover than HadCM3L. This contrast relates to the differences in open ocean SSTs between
238 models. In general, CCSM4 has greater ocean overturning in the high Southern latitudes, which
239 promotes transports of warm equatorial water poleward and inhibits sea ice formation. In
240 contrast, there is less deep-water formation in the high Northern latitudes in either model.
241 Further, the Late Cretaceous Arctic is quite restricted from the greater ocean, especially in the
242 Maa, which prevents warm open ocean waters from having a large effect.

243 Figure DR8. Latitudinal temperature gradient reconstructions from the CEN with the systematic
244 removal of SST proxy reconstruction data from individual methods. Simulated CEN4x zonal
245 average SSTs with all CEN proxies SST except A) foraminifera, B) fish tooth enamel, C) shells
246 and related structures, and D) TEX_{86}. Removal of foraminifera leads to a significantly warmer
247 equator and steeper equator-to-pole temperature gradient. This gradient is steeper than model
248 simulated SSTs. It appears likely that some foraminifera are not recording a pure SST signal.

249 Figure DR9. Latitudinal temperature gradient reconstructions from the MAA with the systematic
250 removal of SST proxy reconstruction data from individual methods. Simulated MAA4x zonal

average SSTs with all MAA proxies SST except A) foraminifera, B) fish tooth enamel, C) shells and related structures, and D) TEX_{86}. Like for the Cen, removal of foraminifera leads to a significantly warmer equator and steeper equator-to-pole temperature gradient.

Figure DR10. Identical to figure S7 except with simulated MAA2x data plotted.

Figure DR11. SST model/proxy discrepancies by latitude. A) Differences between CEN proxies and CEN4x simulations. B) Differences between MAA proxies and MAA4x simulations. C) Differences between MAA proxies and MAA2x simulations. In general, the CEN4x simulations have a cold bias while the MAA4x simulations have a warm bias. The MAA2x simulations are in better agreement with SST proxies. A model warm bias remains in the equatorial region in the MAA2x, but this might be a result of diagenetic alteration of planktonic foramina. While beyond the scope of this work, calibration choices also impact model/proxy agreement. For example, the warmer fish tooth enamel calibration of Pucéat et al. (2010) might result in a better agreement between models and proxies for the MAA2x simulations.

GSA DATA REPOSITORY REFERENCES CITED

Abramovich, S., Keller, G., Stüben, D., and Berner, Z., 2003, Characterization of late Campanian and Maastrichtian planktonic foraminiferal depth habitats and vital activities based on stable isotopes: Palaeogeography Palaeoclimatology Palaeoecology, v. 202, no. 1-2, p. 1–29, doi: 10.1016/S0031-0182(03)00572-8.

Alsenz, H., Regnery, J., Ashckenazi-Polivoda, S., Meilijson, A., Ron-Yankovich, L., Illner, P., Abramovich, S., Almogi-Labin, A., Feinstein, S., Berner, Z., and Püttmann, W., 2013, Characterization of late Campanian and Maastrichtian planktonic foraminiferal depth

habitats and vital activities based on stable isotopes: Palaeogeography Palaeoclimatology Palaeoecology, v. 392, no. C, p. 350–358, doi: 10.1016/j.palaeo.2013.09.013.

Anderson, T.F., Arthur, M.A., 1983: Stable isotopes of oxygen and carbon and their application to sedimentologic and paleoenvironmental problems: Stable Isotopes in Sedimentary Geology, v. 1, p. 1-151.

Ando, A., Nakano, T., Kaiho, K., and Kobayashi, T., 2009, Onset of seawater 87Sr/86Sr excursion prior to Cenomanian–Turonian Oceanic Anoxic Event 2? New Late Cretaceous strontium isotope curve from the central Pacific Ocean: Journal of Foraminiferal Research, v39, no 4, p. 322-334.

Barrera, E., and Savin, S.M., 1999, Evolution of late Campanian-Maastrichtian marine climates and oceans: Geological Society of American-Special Papers, v. 332.

Bemis, E.B., Spero, H.J., Bijma, J., and Lea, D.W., 1998, Reevaluation of the oxygen isotopic composition of planktonic foraminifera: Experimental results and revised paleotemperature equations: Paleoceanography, v. 13, no. 2, p. 150-160.

Bice, K.L., Birgel, D., Meyers, P.A., Dahl, K.A., Hinrichs, K.U., and Norris, R.D., 2006, A multiple proxy and model study of Cretaceous upper ocean temperatures and atmospheric CO_2 concentrations: Paleoceanography, v. 21, no. 2, doi: 10.1029/2005PA001203.

Broecker, W.S., 1989, The Salinity Contrast Between the Atlantic and Pacific Oceans During Glacial Time: Paleoceanography, v. 4, no. 2, p. 207–212, doi: 10.1029/PA004i002p00207.

Carpenter, S.J., Erickson, J.M., and Holland, F.D., 2003, Migration of a Late Cretaceous fish:

293 Nature, v. 423, no. 6935, p. 70–74, doi: 10.1038/nature01588.
294 Clarke, L.J., and Jenkyns, H.C., 1999, New oxygen isotope evidence for long-term Cretaceous
295 climatic change in the Southern Hemisphere: Geology, v. 27, no. 8, p. 699–702.
296 Crowley, T.J., and Zachos, J.C., 2000, Comparison of zonal temperature profiles for past warm
297 time periods: Warm Climates in Earth History, p. 50-76.
298 Cox, P. M., Betts, R. A., Jones, C. D., Spall, S. A., and Totterdell,I. J.:Modelling vegetation and
299 the carbon cycle as interactive elements of the climate system, in: Meteorology at the
300 Millennium, edited by Pearce, R., pp. 259–279, Academic Press, 2001.
301 Damste, J.S.S., van Bentum, E.C., Reichart, G.-J., Pross, J., and Schouten, S., 2010, Earth and
302 Planetary Science Letters: Earth and Planetary Science Letters, v. 293, no. 1-2, p. 97–
303 103, doi: 10.1016/j.epsl.2010.02.027.
304 Davies, A., Kemp, A.E.S., and Pike, J., 2009, Late Cretaceous seasonal ocean variability from
305 the Arctic: Nature, v. 460, no. 7252, p. 254–U118, doi: 10.1038/nature08141.
306 D'Hondt, S., and Lindinger, M., 1994, A stable isotopic record of the Maastrichtian ocean-
307 climate system: South Atlantic DSDP Site 528: Palaeogeography, v. 112, p. 363-378.
308 Ditchfield, P.W., Marshall, J.D., and Pirrie, D., 1994, High latitude palaeotemperature variation:
309 New data from the Thithonian to Eocene of James Ross Island, Antarctica:
310 Palaeogeography, v. 107, p. 79-101.
311 El-Shazly, S., Košťák, M., Kloučková, B., Saber, S.G., Felieh Salama, Y., Mazuch, M., and Žák,
312 K., 2011, Carbon and oxygen stable isotopes of selected Cenomanian and Turonian
313 rudists from Egypt and Czech Republic, and a note on changes in rudist diversity:

Bulletin of Geosciences,, p. 209–226, doi: 10.3140/bull.geosci.1151.

Erez, J., and Luz, B., 1983, Experimental paleotemperature equation for planktonic foraminifera: Geochimica Et Cosmochimica Acta, v. 47, p. 1025-1031.

Frank, T.D., and Arthur, M.A., 1999, Tectonic forcings of Maastrichtian ocean-climate evolution: Paleoceanography, v. 14, no. 2, p. 103–117.

Friedrich, O., Herrle, J.O., Kößler, P., and Hemleben, C., 2004, Early Maastrichtian stable isotopes: changing deep water sources in the North Atlantic?: Palaeogeography Palaeoclimatology Palaeoecology, v. 211, no. 1-2, p. 171–184, doi: 10.1016/j.palaeo.2004.05.004.

Friedrich, O., Erbacher, J., Moriya, K., Wilson, P.A., and Kuhnert, H., 2008, Warm saline intermediate waters in the Cretaceous tropical Atlantic Ocean: Nature Geoscience, v. 1, no. 7, p. 453–457, doi: 10.1038/ngeo217.

Friedrich, O., Herrle, J.O., Wilson, P.A., Cooper, M.J., Erbacher, J., and Hemleben, C., 2009, Early Maastrichtian carbon cycle perturbation and cooling event: Implications from the South Atlantic Ocean: Paleoceanography, v. 24, no. 2, p. n/a–n/a, doi: 10.1029/2008PA001654.

Forster, A., Schouten, S., Baas, M., and Damste, J.S.S., 2007a, Mid-Cretaceous (Albian-Santonian) sea surface temperature record of the tropical Atlantic Ocean: Geology, v. 35, no. 10, p. 919–922, doi: 10.1130/G23874A.1.

Forster, A., Schouten, S., Moriya, K., Wilson, P.A., and Sinninghe Damsté, J.S., 2007b, Tropical warming and intermittent cooling during the Cenomanian/Turonian oceanic anoxic event

335 2: Sea surface temperature records from the equatorial Atlantic: Paleoceanography, v. 22,
336 no. 1, doi: 10.1029/2006PA001349.
337 Gent, P.R., Danabasoglu, G., Donner, L.J., Holland, M.M., Hunke, E.C., Jayne, S.R., Lawrence,
338 D.M., Neale, R.B., Rasch, P.J., Vertenstein, M., Worley, P.H., Yang, Z.-L., and Zhang,
339 M., 2011, The Community Climate System Model Version 4: Journal of Climate, v. 24,
340 no. 19, p. 4973–4991, doi: 10.1175/2011JCLI4083.1.
341 Gordon, C., Cooper, C., Senior, C.A., Banks, H., and Gregory, J.M., 2000, The simulation of
342 SST, sea ice extents and ocean heat transports in a version of the Hadley Centre coupled
343 model without flux adjustments: Climate Dynamics, v. 16, p. 147-168.
344 Gough, D.O., 1981, Solar interior structure and luminosity variations: Physics of Solar
345 Variations, v. 74, p. 21-34.
346 Grossman, E.L., and Ku, T.L., 1986, Oxygen and carbon isotope fractionation in biogenic
347 aragonite: temperature effects: Chemical Geology: Isotope Geoscience section, v. 59; p.
348 59-74.
349 Grossman, E.L., 2012, Reconstructing Earth's deep-time climate-the state of the art in 2012:
350 Paleontological Society Papers, v. 18; p. 39-67.
351 Gustafsson, M., Holbourn, A., and Kuhnt, W., 2003, Changes in Northeast Atlantic temperature
352 and carbon flux during the Cenomanian/Turonian paleoceanographic event: the Goban
353 Spur stable isotope record: Palaeogeography Palaeoclimatology Palaeoecology, v. 201,
354 no. 1-2, p. 51–66, doi: 10.1016/S0031-0182(03)00509-1.
355 Heavens, N.G., Shields, C.A., and Mahowald, N.M., 2012, A paleogeographic approach to

aerosol prescription in simulations of deep time climate: Journal of Advances in Modeling Earth Systems, v. 4, no. 4, p. n/a–n/a, doi: 10.1029/2012MS000166.

Heinemann, M., Jungclaus, J.H., and Marotzke, J., 2009, Warm Paleocene/Eocene climate as simulated in ECHAM5/MPI-OM: Climate of the Past, v. 5, p. 785-802.

Henderson, R.A., and Price, G.D., 2012, Paleoenvironment and paleoecology from oxygen and carbon isotopes of subtropical mollusks from the Late Cretaceous (Cenomanian) of Bathurst Island, Australia: Palaios, v. 27, no. 9, p. 617–626, doi: 10.2110/palo.2011.p11-120r.

Hill, D.J., Haywood, A.M., Lunt, D.J., Hunter, S.J., Bragg, F.J., Contoux, C., Stepanek, C., Sohl, L., Rosenbloom, N.A., Chan, W.L., Kamae, Y., Zhang, Z., Abe-Ouchi, A., Chandler, M.A., et al., 2014, Evaluating the dominant components of warming in Pliocene climate simulations: Climate of the Past, v. 10, no. 1, p. 79–90, doi: 10.5194/cp-10-79-2014.

Huber, B.T., Hodell, D.A., Hamilton, C.P., 1995, Middle–Late Cretaceous climate of the southern high latitudes: stable isotopic evidence for minimal equator-to-pole thermal gradients: Geological Society of America, v. 107, no. 10, p. 1164-1191.

Jenkyns, H.C., Forster, A., Schouten, S., and Damste, J., 2004, High temperatures in the Late Cretaceous Arctic Ocean: Nature, v. 432, no. 7019, p. 888–892, doi: 10.1038/nature03143.

Kim, J.H., van der Meer, J., Schouten, S., Helmke, P., Willmott, V., Sangiorgi, F., Koç, N., Hopmans, E.C., and Damste, J.S.S., 2010, New indices and calibrations derived from the distribution of crenarchaeal isoprenoid tetraether lipids: Implicationsfor past sea surface

temperature reconstructions: Geochimica Et Cosmochimica Acta, v. 74, no. 16, p. 4639–4654, doi: 10.1016/j.gca.2010.05.027.

Kolodny, Y., and Raab, M., 1988, Oxygen isotopes in phosphatic fish remains from Israel: paleothermometry of tropical Cretaceous and Tertiary shelf waters: Palaeogeography, v. 64, p. 59-67.

Kolodny, Y., and Luz, B., 1991, Oxygen isotopes in phosphates of fossil fish—Devonian to Recent: The Geochemical Society, p. 105-119.

Lécuyer, C., Amiot, R., Touzeau, A., and Trotter, J., 2013, Calibration of the phosphate d18O thermometer with carbonate-water oxygen isotope fractionation equations: Chemical Geology, v. 347, no. C, p. 217–226, doi: 10.1016/j.chemgeo.2013.03.008.

Lécuyer, C., Grandjean, P., O'Neil, J.R., and Cappetta, H., 1993, Thermal excursions in the ocean at the Cretaceous—Tertiary boundary (northern Morocco): δ 18 O record of phosphatic fish debris: Palaeogeography, v. 105, p. 235-243.

Levis, S., Bonan, G.B., Vertenstein, M., and Oleson, K.W., 2004, The Community Land Model's Dynamic Global Vegetation Model (CLM-DGVM): Technical Description and User"s Guide: National Center For Atmospheric Research.

Li, L.Q., and Keller, G., 1998, Maastrichtian climate, productivity and faunal turnovers in planktic foraminifera in south Atlantic DSDP sites 525A and 21: Marine Micropaleontology, v. 33, no. 1-2, p. 55–86.

Li, L., and Keller, G., 1999, Variability in Late Cretaceous climate and deep waters: evidence from stable isotopes: Marine Geology, v. 161, p. 171-190.

398 Linnert, C., Robinson, S.A., Lees, J.A., Bown, P.R., guez, I.P.E.R.-R.I., Petrizzo, M.R., Falzoni,
399 F., Littler, K., Arz, J.E.A., and Russell, E.E., 2014, Evidence for global cooling in the
400 Late Cretaceous: Nature Communications, v. 5, p. 1–7, doi: 10.1038/ncomms5194.
401 Lunt, D.J., Dunkley Jones, T., Heinemann, M., Huber, M., LeGrande, A., Winguth, A., Loptson,
402 C., Marotzke, J., Roberts, C.D., Tindall, J., Valdes, P., and Winguth, C., 2012, A model–
403 data comparison for a multi-model ensemble of early Eocene atmosphere–ocean
404 simulations: EoMIP: Climate of the Past, v. 8, no. 5, p. 1717–1736, doi: 10.5194/cp-8-
405 1717-2012-supplement.
406 Lunt, D. J., Farnsworth, A., Loptson, C., Foster, G. L., Markwick, P., O'Brien, C. L., Pancost, R.
407 D., Robinson, S. A., and Wrobel, N., 2016, Palaeogeographic controls on climate and
408 proxy interpretation, Clim. Past., 11, 5683-5725, doi:10.5194/cp-12-1181-2016.
409 Macleod, K.G., Huber, B.T., and Isaza-Londoño, C., 2005, North Atlantic warming during
410 global cooling at the end of the Cretaceous: Geology, v. 33, no. 6, p. 437, doi:
411 10.1130/G21466.1.
412 Maestas, Y., MacLeod, K.G., Douglas, R., Self-Trail, J., and Ward, P.D., 2003, Late Cretaceous
413 foraminifera, paleoenvironments, and paleoceanography of the Rosario Formation, San
414 Antonio del Mar, Baja California, Mexico: Journal of Foraminiferal Research, v. 33, no.
415 3, p. 179–191.
416 Miller, K.G., et al. 2005, The Phanerozoic Record of Global Sea-Level Change: Science, v. 310,
417 no. 5752, p. 1293–1298, doi: 10.1126/science.1116412.
418 Moriya, K., Wilson, P.A., Friedrich, O., Erbacher, J., and Kawahata, H., 2007, Testing for ice

419 sheets during the mid-Cretaceous greenhouse using glassy foraminiferal calcite from the
420 mid-Cenomanian tropics on Demerara Rise: Geology, v. 35, no. 7, p. 615–618, doi:
421 10.1130/G23589A.1.
422 Norris, R.D., and Wilson, P.A., 1998, Low-latitude sea-surface temperatures for the mid-
423 Cretaceous and the evolution of planktic foraminifera: Geology, v. 26, no. 9, p. 832-826.
424 Norris, R.D., Bice, K.L., Magno, E.A., and Wilson, P.A., 2002, Jiggling the tropical thermostat
425 in the Cretaceous hothouse: Geology, v. 30, no. 4, p. 299-302.
426 Ounis, A., Kocsis, L., Chaabani, F., and Pfeifer, H.-R., 2008, Rare earth elements and stable
427 isotope geochemistry (δ13C and δ18O) of phosphorite deposits in the Gafsa Basin,
428 Tunisia: Palaeogeography Palaeoclimatology Palaeoecology, v. 268, no. 1-2, p. 1–18,
429 doi: 10.1016/j.palaeo.2008.07.005.
430 Pearson, P.N., Ditchfield, P.W., Singano, J., Harcourt-Brown, K.G., Nicholas, C.J., Olsson, R.K.,
431 Shackleton, N.J., and Hall, M.A., 2001, Warm tropical sea surface temperatures in the
432 Late Cretaceous and Eocene epochs: Nature, v. 413, no. 6855, p. 481–487.
433 Pirrie, D., and Marshall, J.D., 1990, High-paleolatitude late Cretaceous paleotemperatures: new
434 data from James Ross Island, Antarctica: Geology, v. 18, p. 31-34.
435 Poulsen, C.J., Barron, E.J, Peterson, W.H., and Wilson, P.A.,1999, A reinterpretation of mid-
436 Cretaceous shallow marine temperatures through model-data comparison:
437 Paleoceanography, v. 14, p. 679-697.
438 Price, G.D., Sellwood, B.W., and Corfield, R.M., 1998, Isotopic evidence for palaeotemperatures
439 and depth stratification of Middle Cretaceous planktonic foraminifera from the Pacific

Ocean: Geological Magazine, v. 135, no. 2, p. 183-191.

Price, G.D., and Hart, M.B., 2002, Isotopic evidence for Early to mid-Cretaceous ocean temperature variability: Marine Micropaleontology, v. 46, p. 45-48.

Price, G.D., Williamson, T., Henderson, R.A., and Gagan, M.K., 2012, Barremian-Cenomanian palaeotemperatures for Australian seas based on new oxygen-isotope data from belemnite rostra: Palaeogeography Palaeoclimatology Palaeoecology, v. 358-360, no. C, p. 27–39, doi: 10.1016/j.palaeo.2012.07.015.

Pucéat, E., Joachimski, M.M., Bouilloux, A., Monna, F., Bonin, A., Motreuil, S., Morinière, P., Hénard, S., Mourin, J., Dera, G., and Quesne, D., 2010, Earth and Planetary Science Letters: Earth and Planetary Science Letters, v. 298, no. 1-2, p. 135–142, doi: 10.1016/j.epsl.2010.07.034.

Pucéat, E., Lécuyer, C., Sheppard, S.M.F., Dromart, G., Reboulet, S., and Grandjean, P., 2003, Thermal evolution of Cretaceous Tethyan marine waters inferred from oxygen isotope composition of fish tooth enamels: Paleoceanography, v. 18, no. 2, p. n/a–n/a, doi: 10.1029/2002PA000823.

Pucéat, E., Lécuyer, C., Donnadieu, Y., Naveau, P., Cappetta, H., Ramstein, G., Huber, B.T., and Kriwet, J., 2007, Fish tooth δ18O revising Late Cretaceous meridional upper ocean water temperature gradients: Geology, v. 35, no. 2, p. 107, doi: 10.1130/G23103A.1.

Schönfeld, J., Sirocko, F., and Jørgensen, N.O., 1991, Oxygen isotope composition of Upper Cretaceous chalk at Lägerdorf (NW Germany): its original environmental signal and palaeotemperature interpretation: Cretaceous Research, v.12, p. 27-46.

461 Sellwood, B.W., Price, G.D., and Valdest, P.J., 1994, Cooler estimates of Cretaceous
462 temperatures: Nature, v. 370, p. 453-455.
463 Schouten, S., Hopmans, E.C., Schefuss, E., and Damste, J., 2002, Distributional variations in
464 marine crenarchaeotal membrane lipids: a new tool for reconstructing ancient sea water
465 temperatures?: Earth and Planetary Science Letters, v. 204, no. 1-2, p. 265–274.
466 Schouten, S., Hopmans, E.C., Forster, A., van Breugel, Y., Kuypers, M.M.M., and Sinninghe
467 Damsté, J.S., 2003, Extremely high sea-surface temperatures at low latitudes during the
468 middle Cretaceous as revealed by archaeal membrane lipids: Geology, v. 31, no. 12, p.
469 1069, doi: 10.1130/G19876.1.
470 Spicer, R.A., and Herman, A.B., 2010, The Late Cretaceous environment of the Arctic: A
471 quantitative reassessment based on plant fossils: Palaeogeography Palaeoclimatology
472 Palaeoecology, v. 295, no. 3-4, p. 423–442, doi: 10.1016/j.palaeo.2010.02.025.
473 Steuber, T., Rauch, M., Masse, J.P., Graaf, J., and Malkoč, M., 2005, Low-latitude seasonality of
474 Cretaceous temperatures in warm and cold episodes: Nature, v. 437, no. 7063, p. 1341–
475 1344, doi: 10.1038/nature04096.
476 Taylor, K.W.R., Huber, M., Hollis, C.J., Hernandez-Sanchez, M.T., and Pancost, R.D., 2013,
477 Global and Planetary Change: Global and Planetary Change, v. 108, no. C, p. 158–174,
478 doi: 10.1016/j.gloplacha.2013.06.011.
479 Upchurch, G.R., Otto-Bliesner, B.L., and Scotese, C., 1998, Vegetation–atmosphere interactions
480 and their role in global warming during the latest Cretaceous: Philosophical Transactions
481 of the Royal Society of London B, v. 353, p. 97-112.

Upchurch, G.R., Jr, Kiehl, J., Shields, C., Scherer, J., and Scotese, C., 2015, Latitudinal temperature gradients and high-latitude temperatures during the latest Cretaceous: Congruence of geologic data and climate models: Geology, v. 43, no. 8, p. 683–686, doi: 10.1130/G36802.1.

Vellekoop, J., Sluijs, A., Smit, J., Schouten, S., Weijers, J.W.H., Sinninghe Damste, J.S., and Brinkhuis, H., 2014, Rapid short-term cooling following the Chicxulub impact at the Cretaceous-Paleogene boundary: Proceedings of the National Academy of Sciences, v. 111, no. 21, p. 7537–7541, doi: 10.1073/pnas.1319253111.

Voigt, S., Wilmsen, M., Mortimore, R.N., and Voigt, T., 2003, Cenomanian palaeotemperatures derived from the oxygen isotopic composition of brachiopods and belemnites: evaluation of Cretaceous palaeotemperature proxies: International Journal of Earth Science. doi: 10.1007/s00531-003-0315-1.

Voigt, S., Gale, A.S., and Flögel, S., 2004, Midlatitude shelf seas in the Cenomanian-Turonian greenhouse world: Temperature evolution and North Atlantic circulation: Paleoceanography, v. 19, no. 4,, doi: 10.1029/2004PA001015.

Wilson, P.A., and Opdyke, B.N., 1996, Equatorial sea-surface temperatures for the Maastrichtian revealed through remarkable preservation of metastable carbonate: Geology, v. 24, no. 6, p. 555-558.

Zachos, J.C., Stott, L.D., and Lohmann, K.C., 1994, Evolution of early Cenozoic marine temperatures: Paleoceanography, v. 9, no. 2, p. 353-387.

Zakharov, Y.D., Popov, A.M., and Shigeta, Y., 2006, New Maastrichtian oxygen and carbon

isotope record: additional evidence for warm low latitudes: Geosciences Journal, v. 10, no. 3, p. 347-367.

Zhou, J., Poulsen, C.J., pollard, D., and White, T.S., 2008, Simulation of modern and middle Cretaceous marine delta O-18 with an ocean-atmosphere general circulation model: Paleoceanography, v. 23, no. 3, doi: 10.1029/2008PA001596.

Cenomanian Paleogeography and Proxy Locations

Fig. DR1

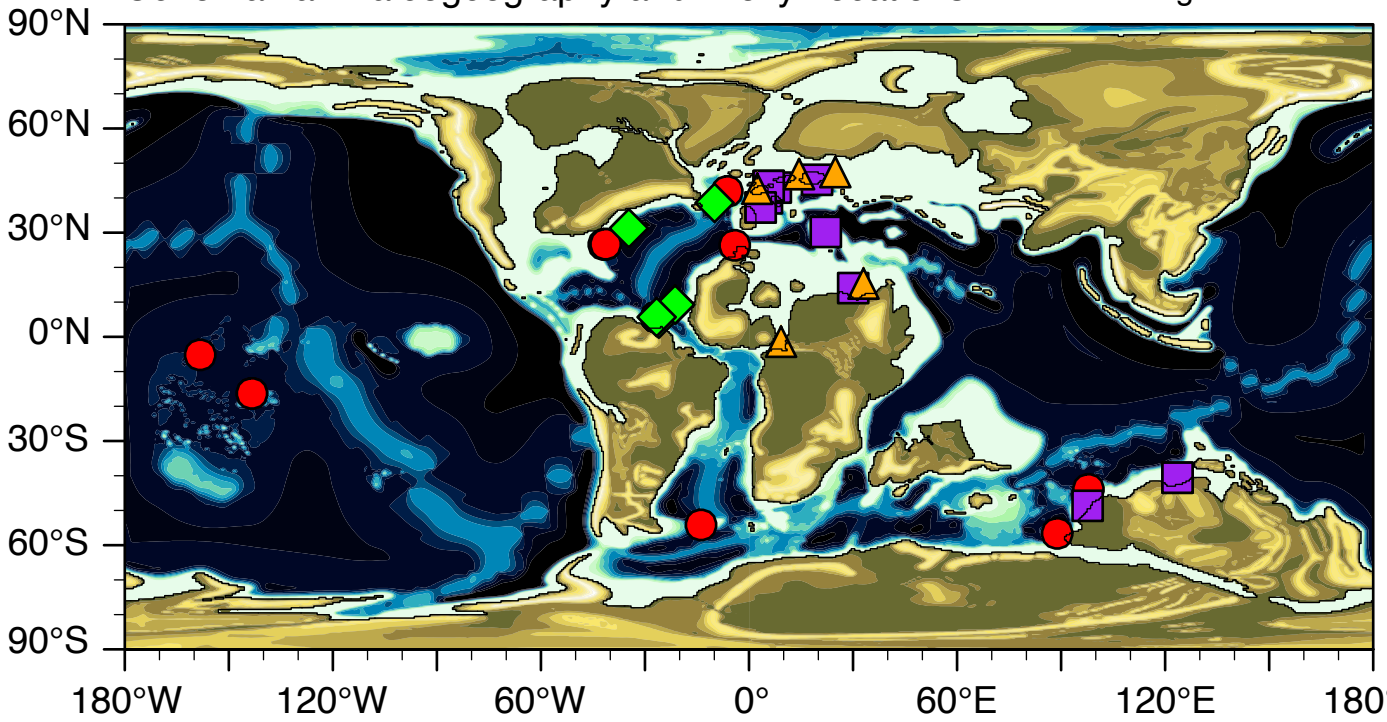

Maastrichtian Paleogeography and Proxy Locations

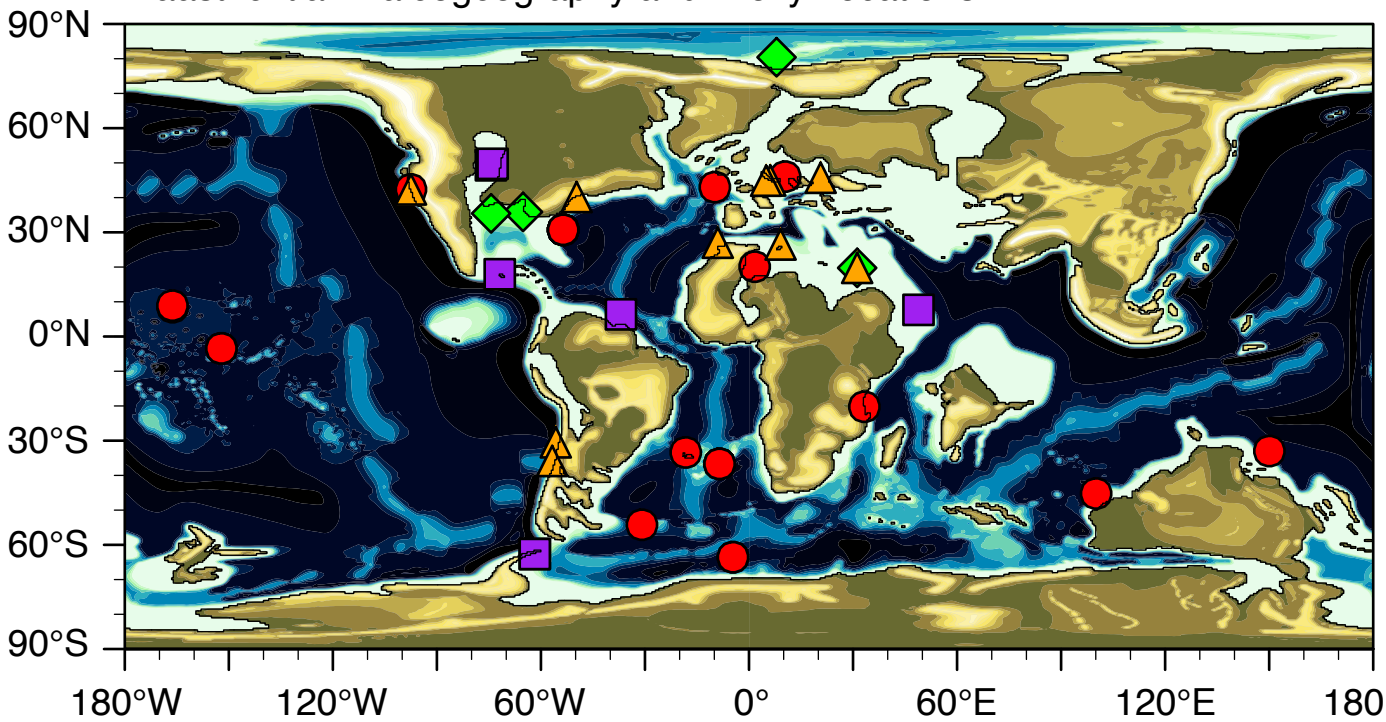

Shells
Foram
Teeth
TEX_{86}

-5000 -2500 0 2500 5000

Meters Above Sea Level

Fig. DR2

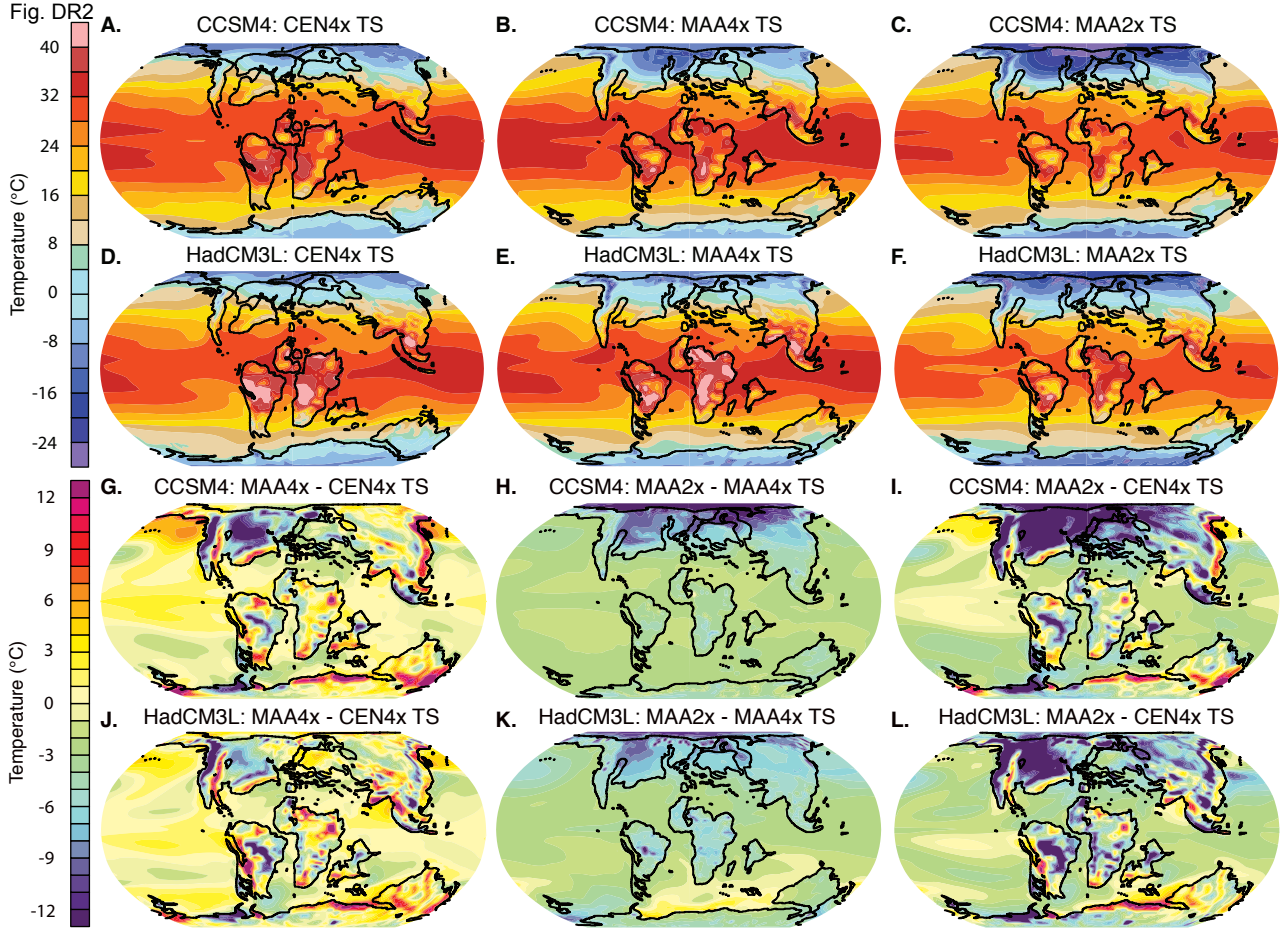
A. CCSM4: CEN4x TS
B. CCSM4: MAA4x TS
C. CCSM4: MAA2x TS
D. HadCM3L: CEN4x TS
E. HadCM3L: MAA4x TS
F. HadCM3L: MAA2x TS
Temperature (°C)
40
32
24
16
8
0
-8
-16
-24
G. CCSM4: MAA4x - CEN4x TS
H. CCSM4: MAA2x - MAA4x TS
I. CCSM4: MAA2x - CEN4x TS
J. HadCM3L: MAA4x - CEN4x TS
K. HadCM3L: MAA2x - MAA4x TS
L. HadCM3L: MAA2x - CEN4x TS
Temperature (°C)
12
9
6
3
0
-3
-6
-9
-12

Fig. DR3

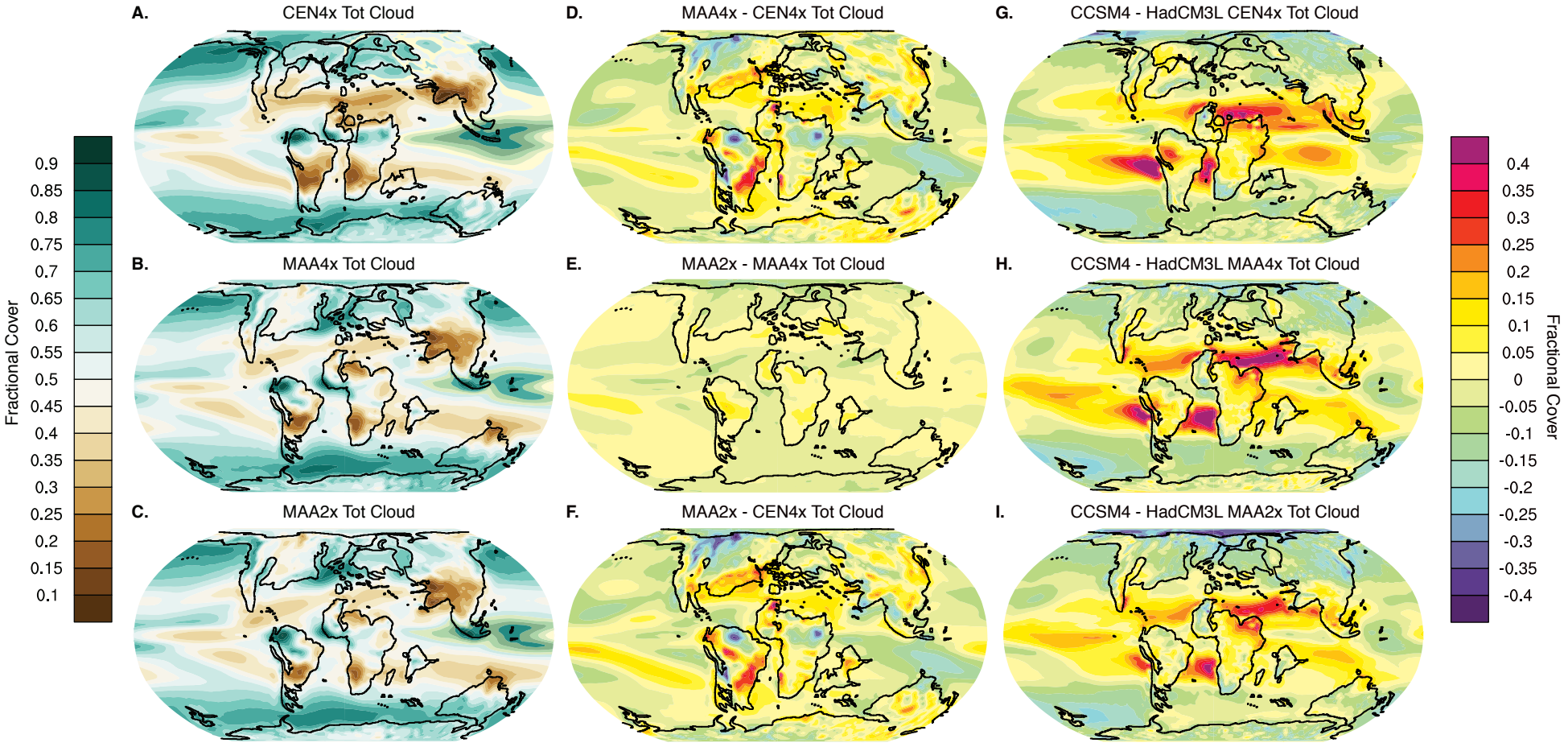
A.
CEN4x Tot Cloud
B.
MAA4x Tot Cloud
C.
MAA2x Tot Cloud
D.
MAA4x - CEN4x Tot Cloud
E.
MAA2x - MAA4x Tot Cloud
F.
MAA2x - CEN4x Tot Cloud
G.
CCSM4 - HadCM3L CEN4x Tot Cloud
H.
CCSM4 - HadCM3L MAA4x Tot Cloud
I.
CCSM4 - HadCM3L MAA2x Tot Cloud
Fractional Cover
0.9
0.85
0.8
0.75
0.7
0.65
0.6
0.55
0.5
0.45
0.4
0.35
0.3
0.25
0.2
0.15
0.1
Fractional Cover
0.4
0.35
0.3
0.25
0.2
0.15
0.1
0.05
0
-0.05
-0.1
-0.15
-0.2
-0.25
-0.3
-0.35
-0.4

Fig. DR4

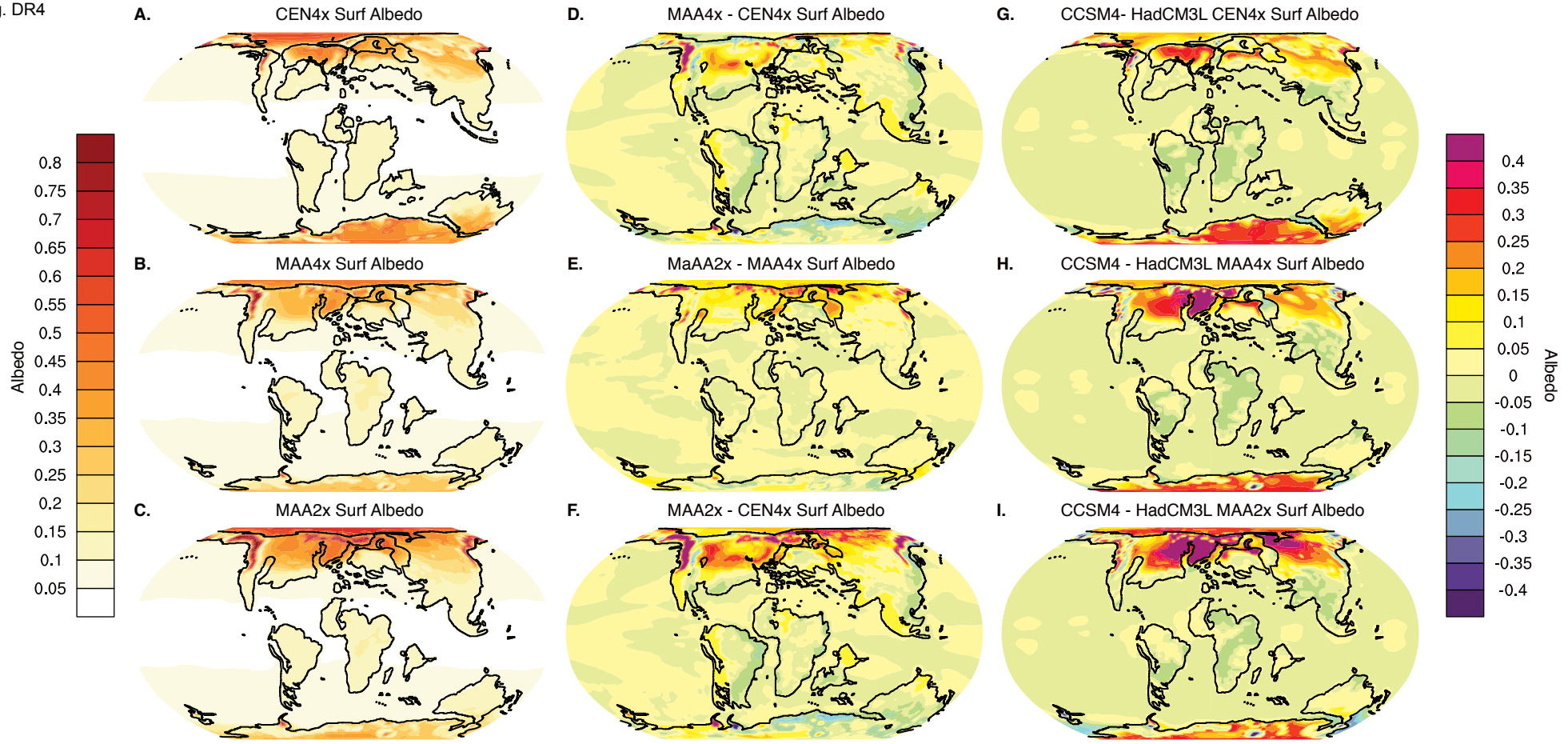
A.
CEN4x Surf Albedo
B.
MAA4x Surf Albedo
C.
MAA2x Surf Albedo
D.
MAA4x - CEN4x Surf Albedo
E.
MaAA2x - MAA4x Surf Albedo
F.
MAA2x - CEN4x Surf Albedo
G.
CCSM4- HadCM3L CEN4x Surf Albedo
H.
CCSM4 - HadCM3L MAA4x Surf Albedo
I.
CCSM4 - HadCM3L MAA2x Surf Albedo
Albedo
0.8
0.75
0.7
0.65
0.6
0.55
0.5
0.45
0.4
0.35
0.3
0.25
0.2
0.15
0.1
0.05
Albedo
0.4
0.35
0.3
0.25
0.2
0.15
0.1
0.05
0
-0.05
-0.1
-0.15
-0.2
-0.25
-0.3
-0.35
-0.4

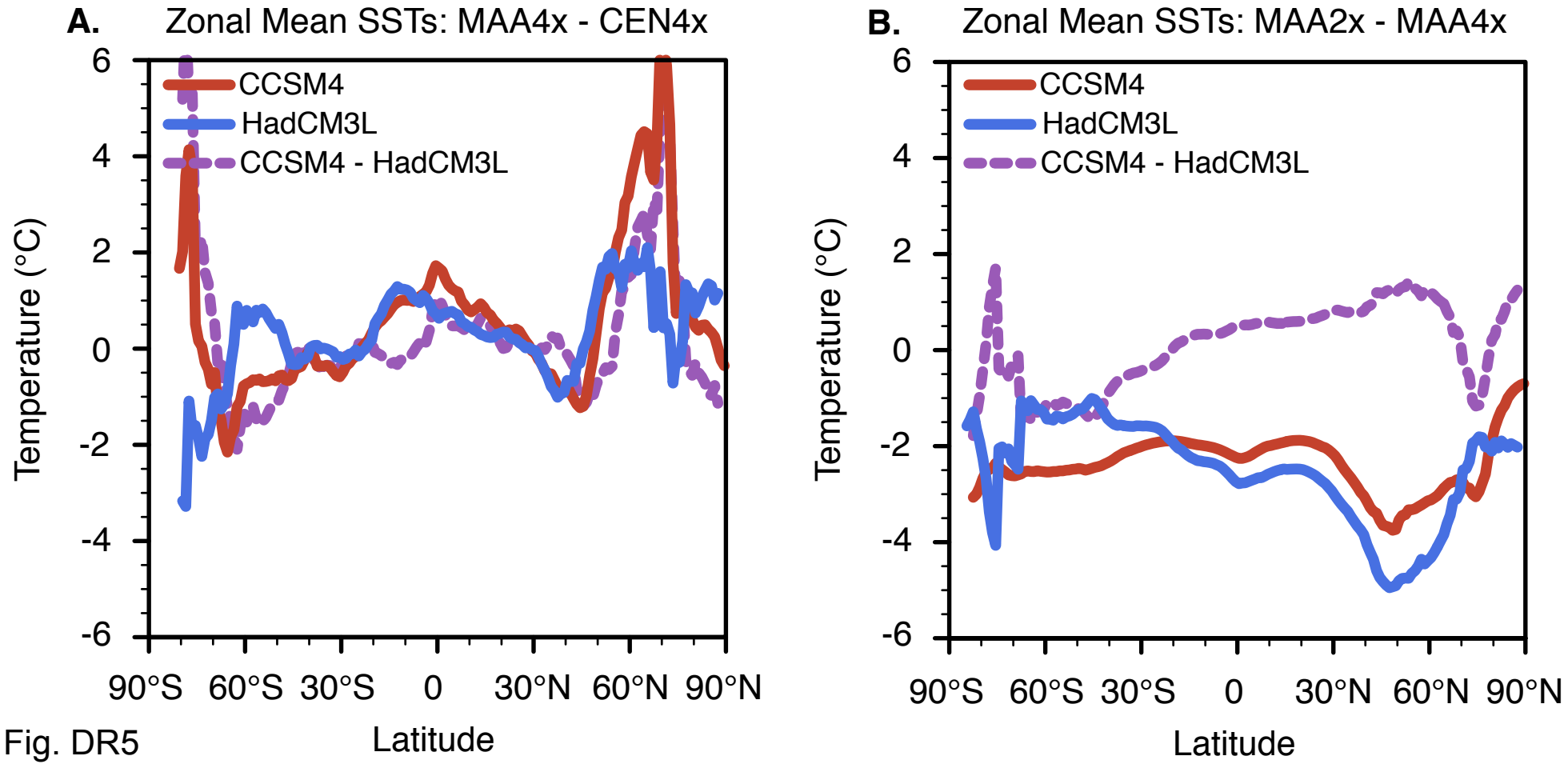
A.
Zonal Mean SSTs: MAA4x - CEN4x
CCSM4
HadCM3L
CCSM4 - HadCM3L
Temperature (°C)
6
4
2
0
-2
-4
-6
90°S
60°S
30°S
0
30°N
60°N
90°N
Latitude
B.
Zonal Mean SSTs: MAA2x - MAA4x
CCSM4
HadCM3L
CCSM4 - HadCM3L
Temperature (°C)
6
4
2
0
-2
-4
-6
90°S
60°S
30°S
0
30°N
60°N
90°N
Latitude

Fig. DR5

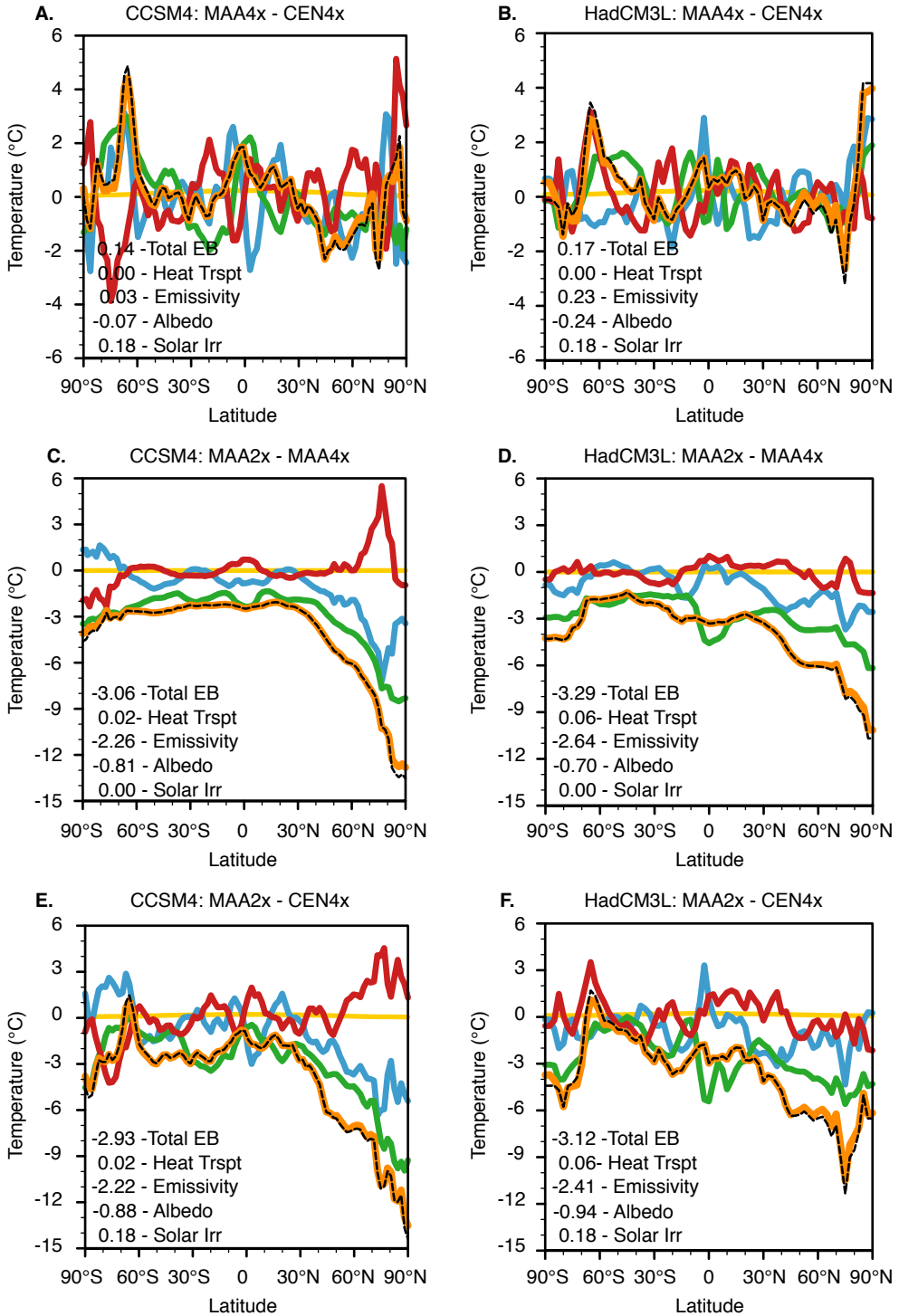
A.
CCSM4: MAA4x - CEN4x
0.14 -Total EB
0.00 - Heat Trspt
0.03 - Emissivity
-0.07 - Albedo
0.18 - Solar Irr
B.
HadCM3L: MAA4x - CEN4x
0.17 -Total EB
0.00 - Heat Trspt
0.23 - Emissivity
-0.24 - Albedo
0.18 - Solar Irr
C.
CCSM4: MAA2x - MAA4x
-3.06 -Total EB
0.02- Heat Trspt
-2.26 - Emissivity
-0.81 - Albedo
0.00 - Solar Irr
D.
HadCM3L: MAA2x - MAA4x
-3.29 -Total EB
0.06- Heat Trspt
-2.64 - Emissivity
-0.70 - Albedo
0.00 - Solar Irr
E.
CCSM4: MAA2x - CEN4x
-2.93 -Total EB
0.02 - Heat Trspt
-2.22 - Emissivity
-0.88 - Albedo
0.18 - Solar Irr
F.
HadCM3L: MAA2x - CEN4x
-3.12 -Total EB
0.06- Heat Trspt
-2.41 - Emissivity
-0.94 - Albedo
0.18 - Solar Irr
Temperature (°C)
Latitude
90°S 60°S 30°S 0 30°N 60°N 90°N
Actual
Heat Trspt
Albedo
Total EB
Emissivity
Solar Irr

Fig. DR6

A. CEN4x Ann Avg Sea Ice: CCSM4 NH

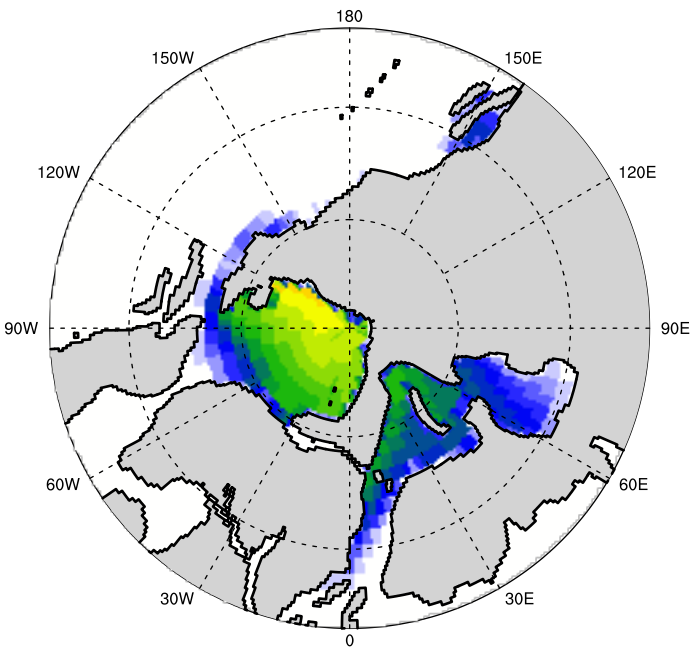

B. CEN4x Ann Avg Sea Ice: HadCM3L NH

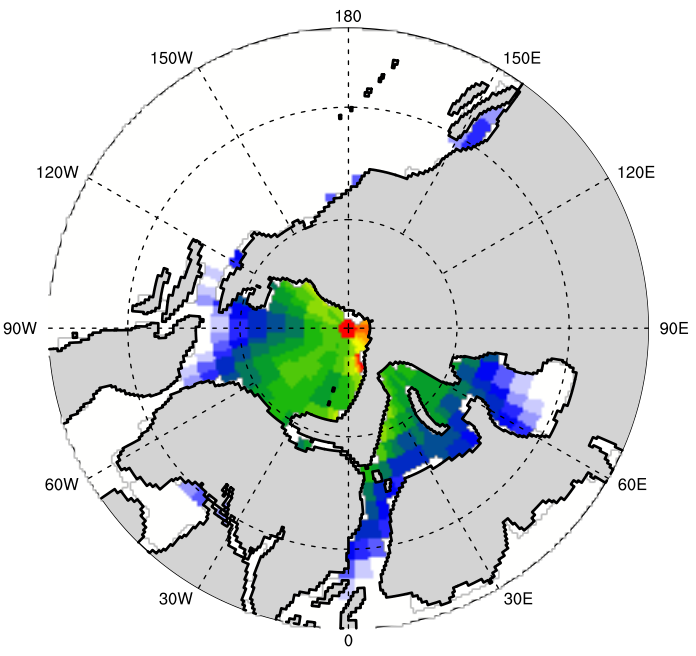

C. CEN4x Ann Avg Sea Ice: CCSM4 SH

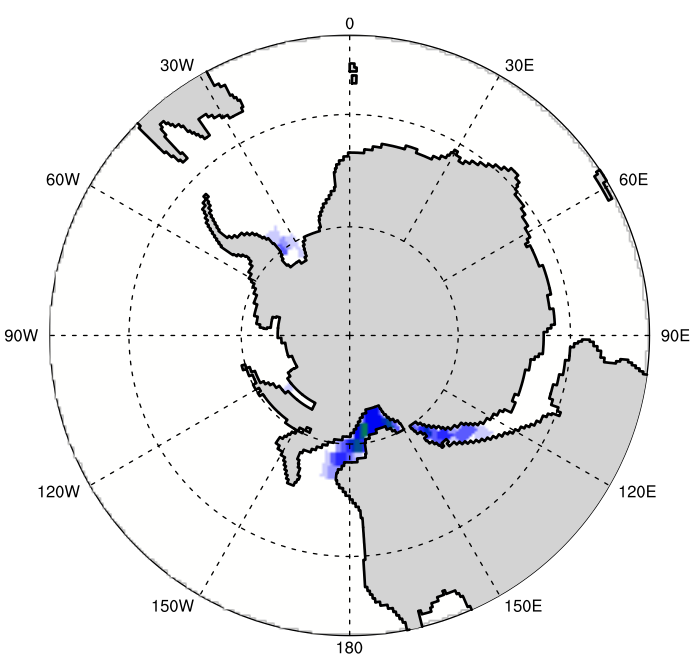

D. CEN4x Ann Avg Sea Ice: HadCM3L SH

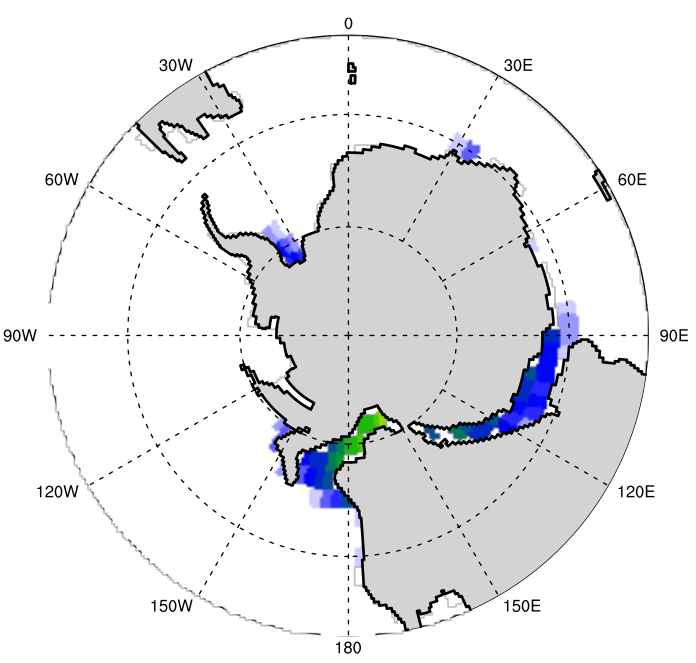

E. MAA4x Ann Avg Sea Ice: CCSM4 NH

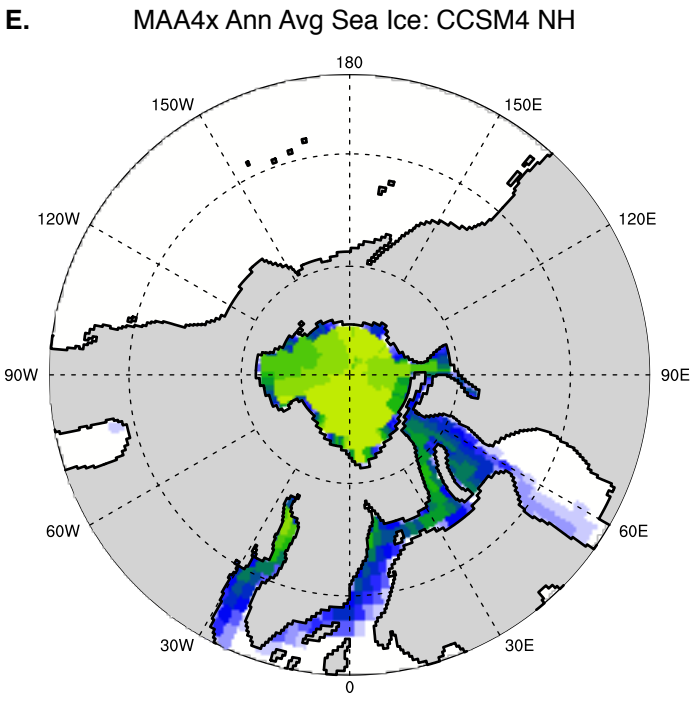

F. MAA4x Ann Avg Sea Ice: HadCM3L NH

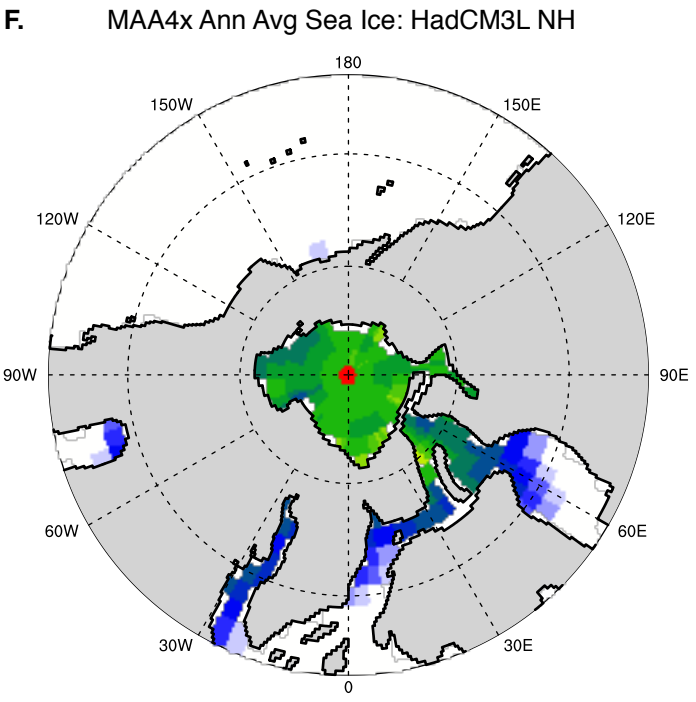

G. MAA4x Ann Avg Sea Ice: CCSM4 SH

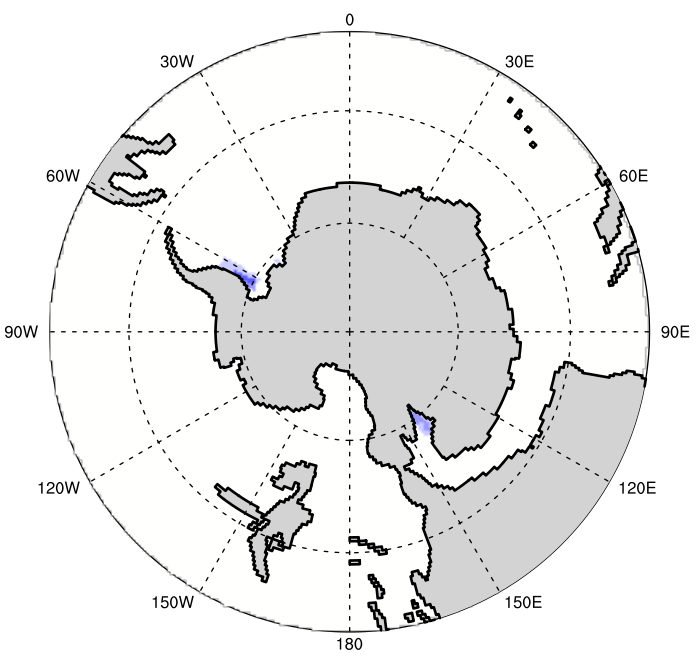

H. MAA4x Ann Avg Sea Ice: HadCM3L SH

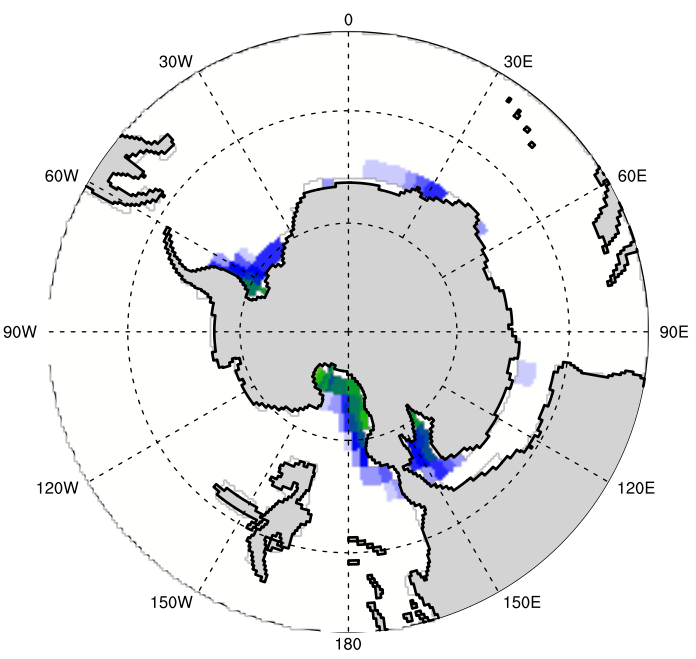

I. MAA2x Ann Avg Sea Ice: CCSM4 NH

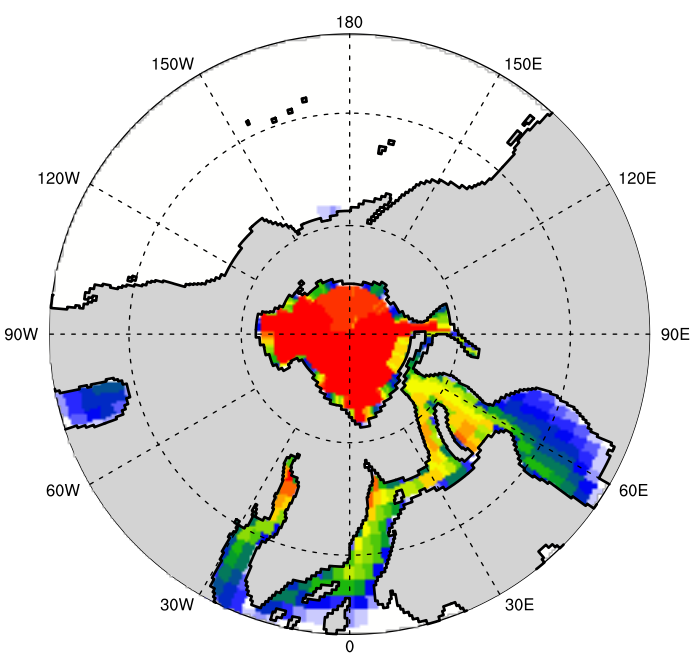

J. MAA2x Ann Avg Sea Ice: HadCM3L NH

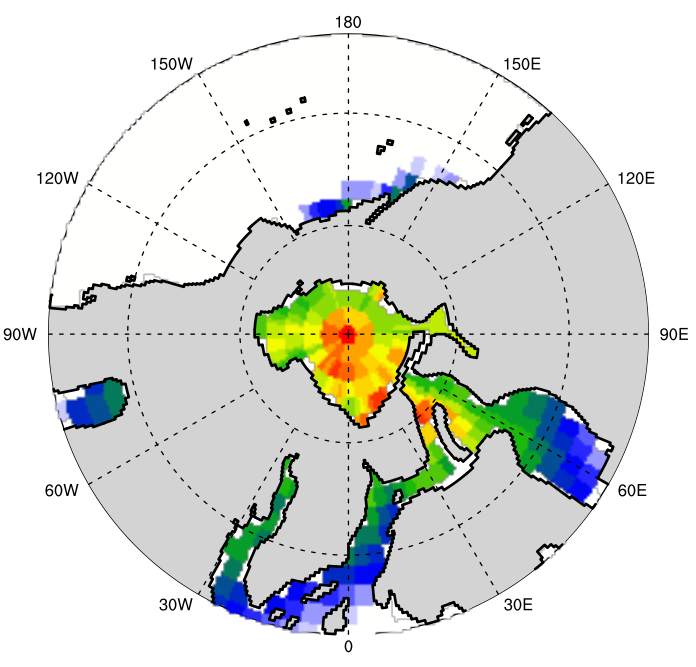

K. MAA2x Ann Avg Sea Ice: CCSM4 SH

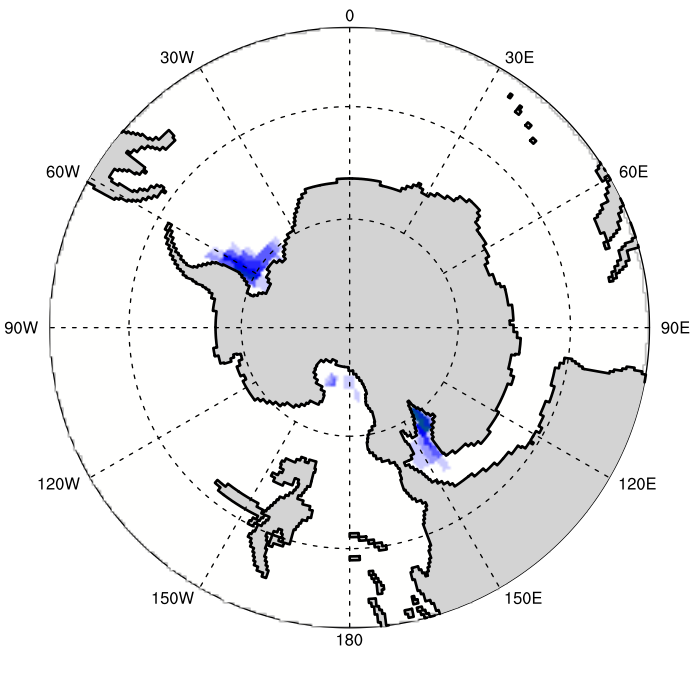

L. MAA2x Ann Avg Sea Ice: HadCM3L SH

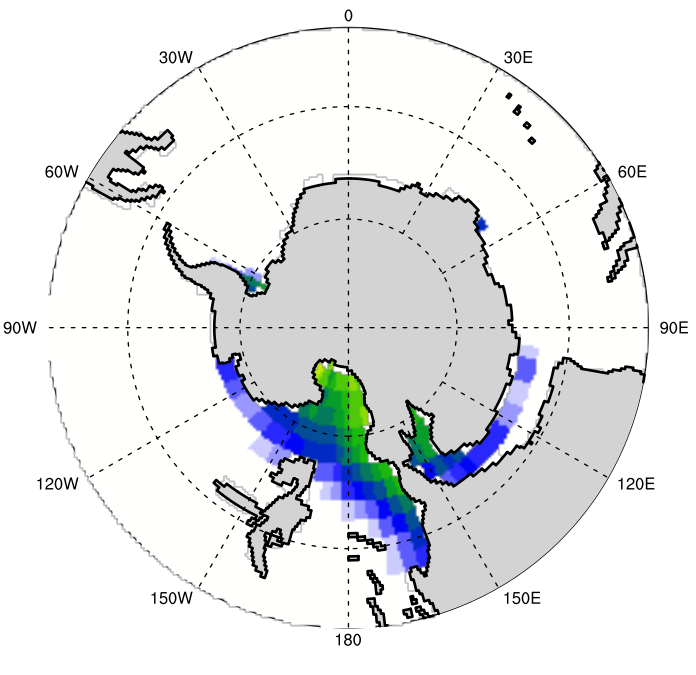

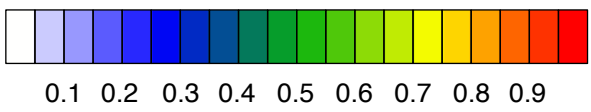

Fig. DR7

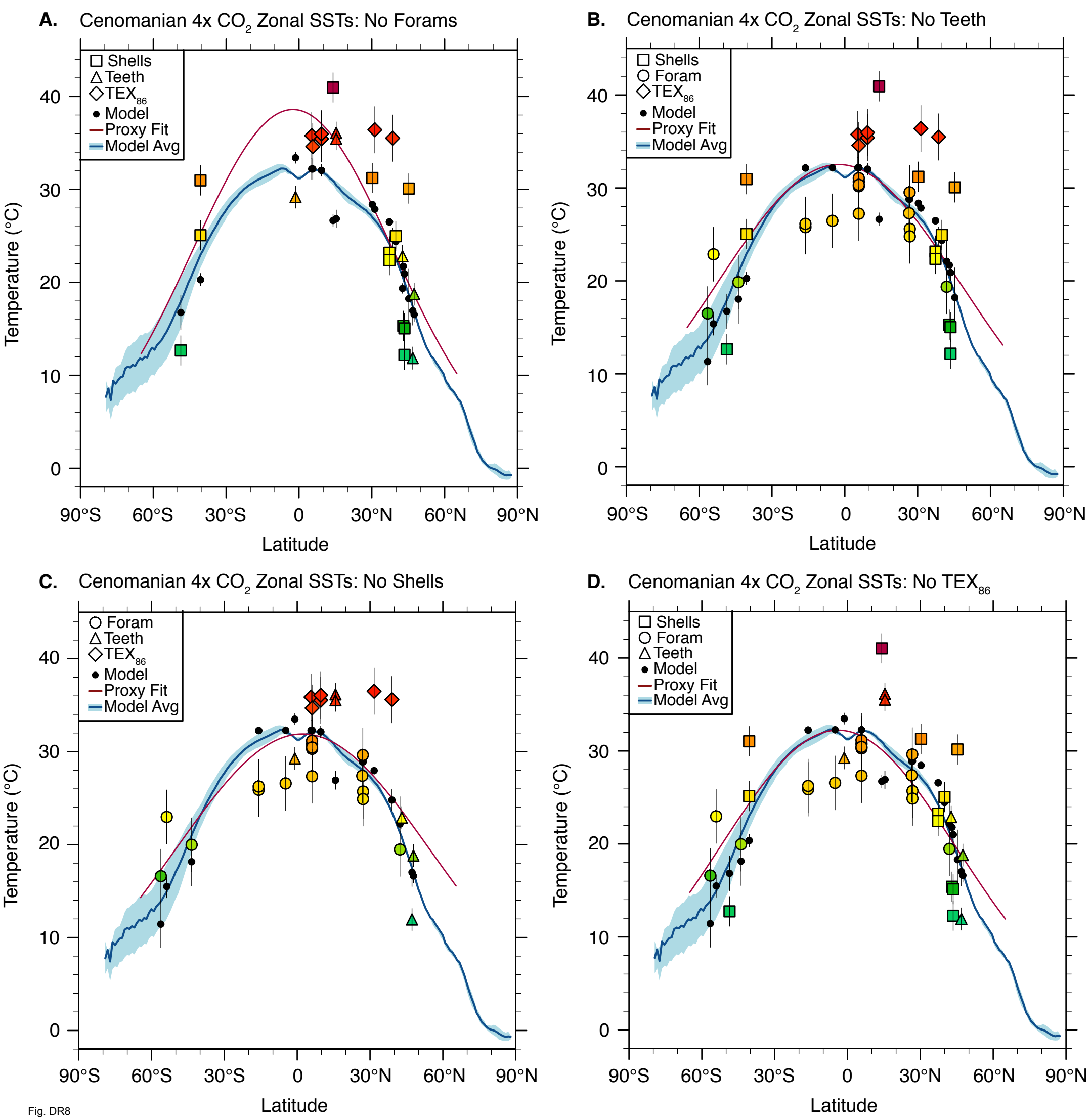
A. Cenomanian 4x CO2 Zonal SSTs: No Forams
Shells
Teeth
TEX86
Model
Proxy Fit
Model Avg
Temperature (°C)
0
10
20
30
40
90°S
60°S
30°S
0
30°N
60°N
90°N
Latitude
B. Cenomanian 4x CO2 Zonal SSTs: No Teeth
Shells
Foram
TEX86
Model
Proxy Fit
Model Avg
Temperature (°C)
Latitude
C. Cenomanian 4x CO2 Zonal SSTs: No Shells
Foram
Teeth
TEX86
Model
Proxy Fit
Model Avg
Temperature (°C)
Latitude
D. Cenomanian 4x CO2 Zonal SSTs: No TEX86
Shells
Foram
Teeth
Model
Proxy Fit
Model Avg
Temperature (°C)
Latitude

Fig. DR8

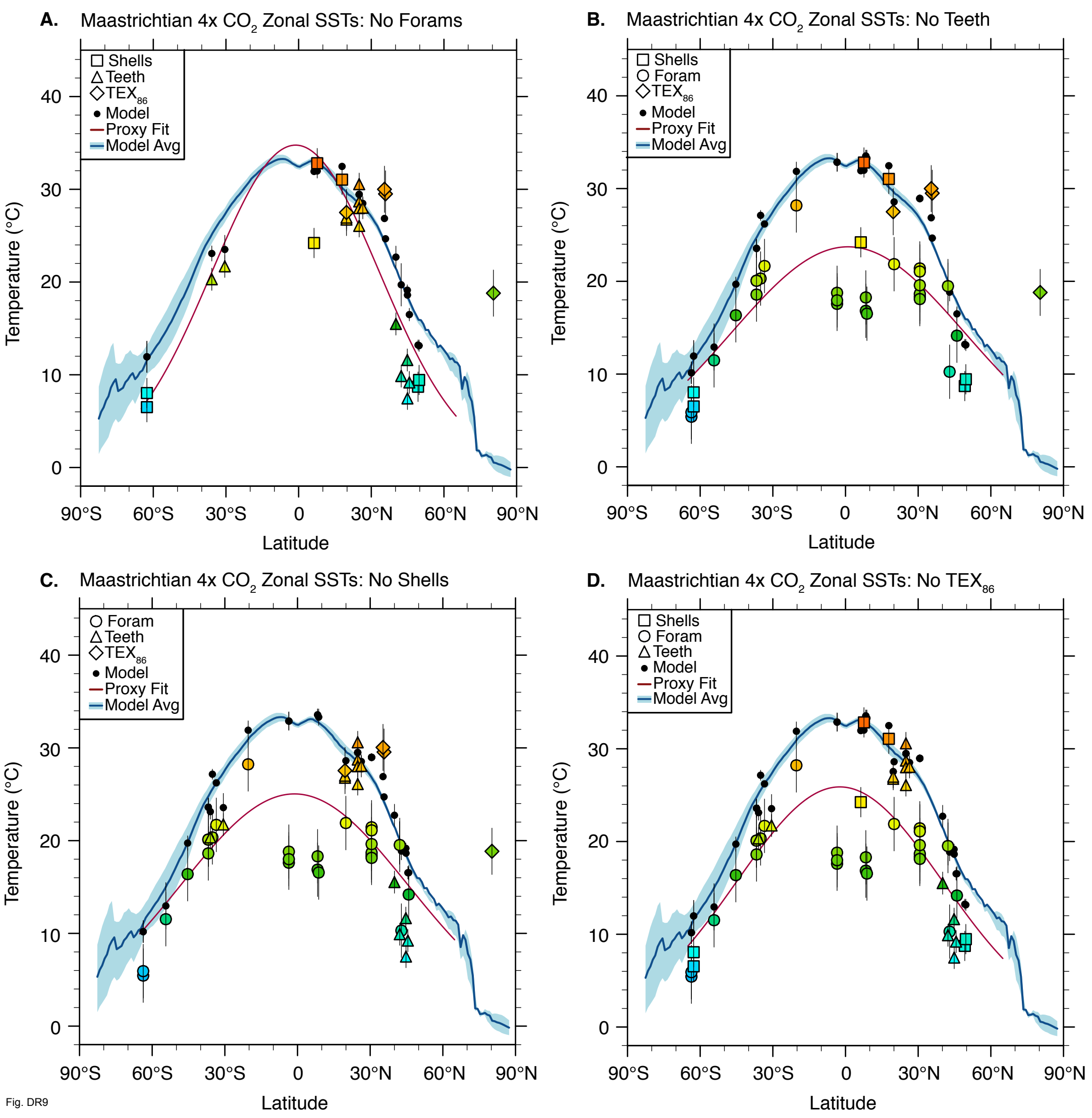
A. Maastrichtian 4x CO2 Zonal SSTs: No Forams
Shells
Teeth
TEX86
Model
Proxy Fit
Model Avg
B. Maastrichtian 4x CO2 Zonal SSTs: No Teeth
Shells
Foram
TEX86
Model
Proxy Fit
Model Avg
C. Maastrichtian 4x CO2 Zonal SSTs: No Shells
Foram
Teeth
TEX86
Model
Proxy Fit
Model Avg
D. Maastrichtian 4x CO2 Zonal SSTs: No TEX86
Shells
Foram
Teeth
Model
Proxy Fit
Model Avg
Temperature (°C)
0
10
20
30
40
90°S
60°S
30°S
0
30°N
60°N
90°N
Latitude

Fig. DR9

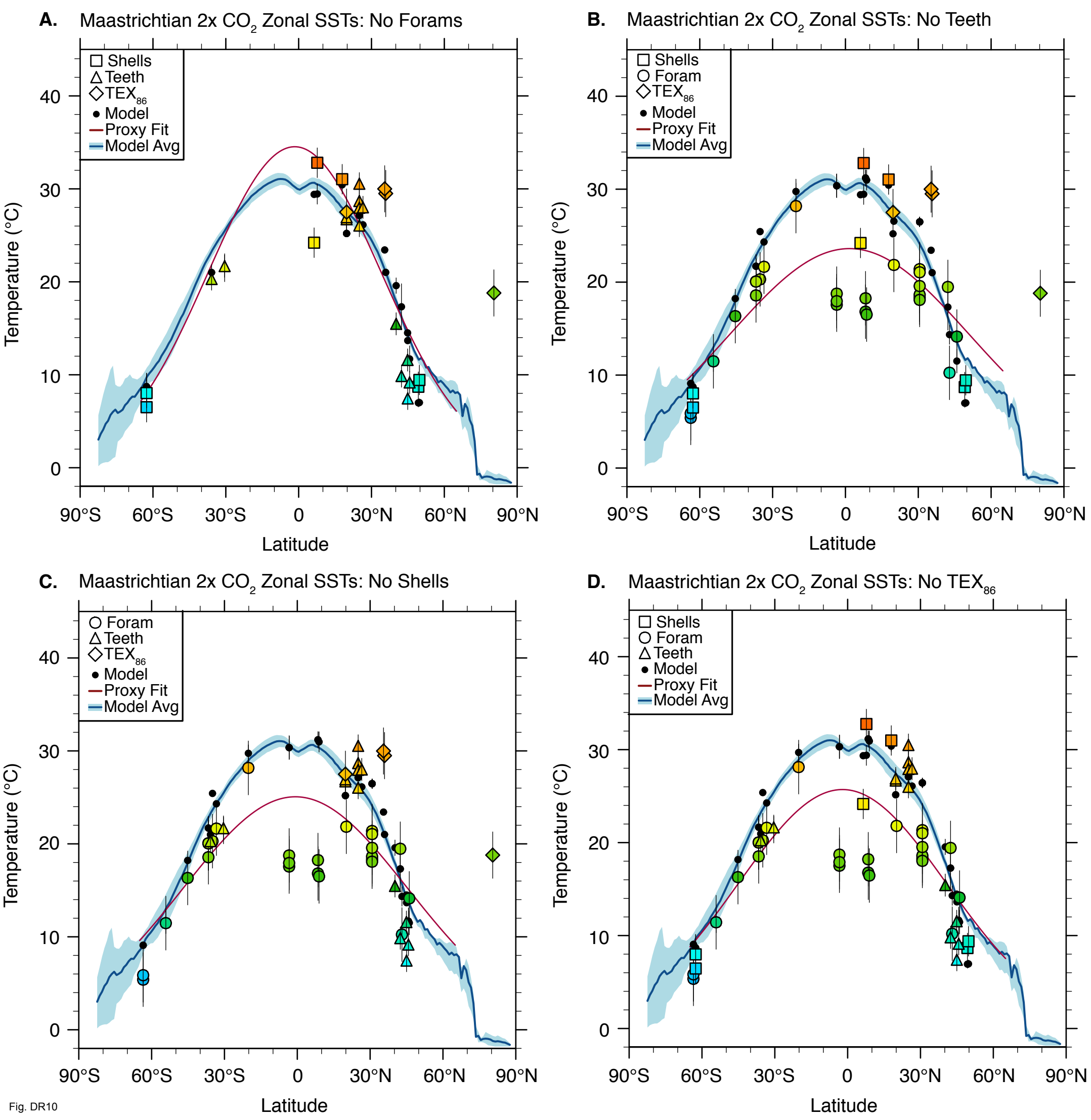
A. Maastrichtian 2x CO2 Zonal SSTs: No Forams
Shells
Teeth
TEX86
Model
Proxy Fit
Model Avg
Temperature (°C)
0
10
20
30
40
90°S
60°S
30°S
0
30°N
60°N
90°N
Latitude
B. Maastrichtian 2x CO2 Zonal SSTs: No Teeth
Shells
Foram
TEX86
Model
Proxy Fit
Model Avg
Temperature (°C)
Latitude
C. Maastrichtian 2x CO2 Zonal SSTs: No Shells
Foram
Teeth
TEX86
Model
Proxy Fit
Model Avg
Temperature (°C)
Latitude
D. Maastrichtian 2x CO2 Zonal SSTs: No TEX86
Shells
Foram
Teeth
Model
Proxy Fit
Model Avg
Temperature (°C)
Latitude

Fig. DR10

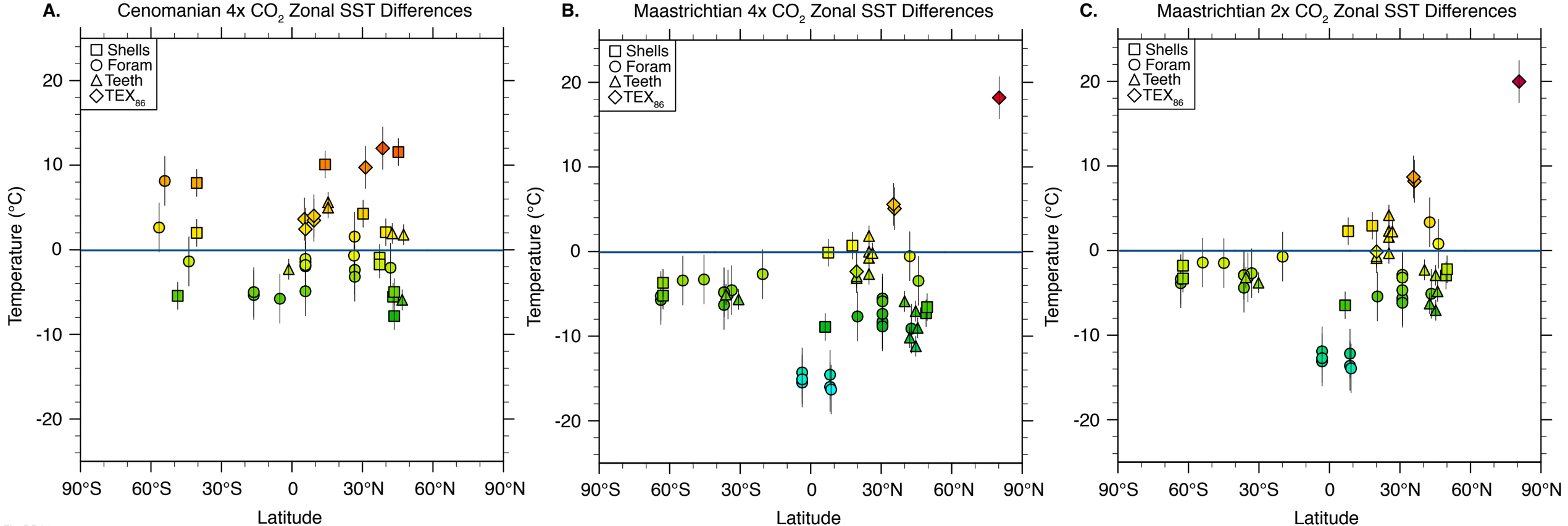
A.
Cenomanian 4x CO2 Zonal SST Differences
B.
Maastrichtian 4x CO2 Zonal SST Differences
C.
Maastrichtian 2x CO2 Zonal SST Differences
Shells
Foram
Teeth
TEX86
Temperature (°C)
20
10
0
-10
-20
90°S
60°S
30°S
0
30°N
60°N
90°N
Latitude

Fig. DR11

TABLE DR1: MODEL CONFIGURATION AND DATA

Experiment	Age (Ma)	Solar Constant (Wm^{-2})	CO_2 (ppmv)	Global MAT (°C)	EQ Temp: 5°S-5°N (°C)	N Pole Temp: 85°-90°N (°C)	S Pole Temp: 85°-90°S (°C)	NH Gradient (°C)	SH Gradient (°C)
Cen4x: CESM	96.4	1353.9	1120	22.80093	30.75579	-10.93816	-4.673659	41.69395	35.429449
Cen4x: HadCM3L	96.4	1353.9	1120	22.17896	31.68976	-12.16977	-7.613354	43.85953	39.303114
Maa4x: CESM	68.2	1357.18	1120	22.92284	31.92628	-9.934456	-5.359563	41.860736	37.285843
Maa4x: HadCM3L	68.2	1357.18	1120	22.33742	32.52404	-8.000755	-7.752418	40.524795	40.276458
Maa2x: CESM	68.2	1357.18	560	19.81563	29.51464	-23.30825	-9.552328	52.82289	39.066968
Maa2x: HadCM3L	68.2	1357.18	560	19.02272	29.29172	-18.09064	-12.0258	47.38236	41.31752

Note: All reported temperatures are mean annual surface temperatures.

TABLE DR2: ALL MAASTRICHTIAN AND CENOMANIAN SST DATA